

1 **Sustainable Production of the Biofuel *n*-Butanol by *Rhodopseudomonas***
2 ***palustris* TIE-1**

3 W. Bai², T. O. Ranaivoarisoa¹, R. Singh¹, K. Rengasamy¹, A. Bose^{1*}

4
5 ¹Department of Biology, Washington University in St. Louis, St. Louis, MO, USA.

6 ²Department of Energy, Environmental and Chemical Engineering, Washington University in St.
7 Louis, St. Louis, MO, USA.

8
9 *Corresponding author: Arpita Bose, Department of Biology, Washington University in
10 St. Louis, One Brookings Drive, St. Louis, 63130

11 Email: abose@wustl.edu

12 Phone: +1-314-935-6236

13 Fax: +1-314-935-443

14
15 *Keywords:* *Rhodopseudomonas palustris TIE-1; Metabolic engineering; Microbial*
16 *electrosynthesis; Solar fuels; Carbon-neutral; n-Butanol*

17 **Abstract**

18 Anthropogenic carbon dioxide (CO₂) release in the atmosphere from fossil fuel combustion has
19 inspired scientists to study CO₂ to fuel conversion. Oxygenic phototrophs such as cyanobacteria
20 have been used to produce biofuels using CO₂. However, oxygen generation during oxygenic
21 photosynthesis affects biofuel production efficiency. To produce *n*-butanol (biofuel) from CO₂,
22 here we introduced an *n*-butanol biosynthesis pathway into an anoxygenic (non-oxygen evolving)
23 photoautotroph, *Rhodospseudomonas palustris* TIE-1 (TIE-1). Using different carbon, nitrogen,
24 and electron sources, we achieved *n*-butanol production in wild-type TIE-1 and mutants lacking
25 electron-consuming (nitrogen-fixing) or acetyl-CoA-consuming (polyhydroxybutyrate and
26 glycogen synthesis) pathways. The mutant lacking the nitrogen-fixing pathway produced highest
27 *n*-butanol. Coupled with novel hybrid bioelectrochemical platforms, this mutant produced *n*-
28 butanol using CO₂, solar panel-generated electricity, and light, with high electrical energy
29 conversion efficiency. Overall, this approach showcases TIE-1 as an attractive microbial chassis
30 for carbon-neutral *n*-butanol bioproduction using sustainable, renewable, and abundant resources.

31

32

33 **Introduction**

34 The rapid consumption of fossil fuels has increased carbon dioxide (CO₂) levels in the atmosphere
35 raising concerns about global warming^{1,2}. This environmental concern has spurred research
36 initiatives aiming to develop carbon-neutral biofuels that, when burned, will not result in net CO₂
37 release³. Among the various biofuels, *n*-butanol has received greater attention due to its higher
38 energy content, lower volatility, and reduced hydrophilicity compared to ethanol⁴. Currently, most
39 *n*-butanol is synthesized via chemical processes^{5,6}. However, these processes use propylene or
40 ethanol as feedstock, making these methods, carbon-positive^{5,6}. Another well-known strategy for
41 *n*-butanol production is the acetone–butanol–ethanol (ABE) fermentation using *Clostridium*
42 species⁷. As such, the *n*-butanol biosynthesis pathway⁷ (Fig. 1a) from *Clostridium acetobutylicum*
43 has been introduced into several organisms, such as *Escherichia coli*, *Saccharomyces cerevisiae*,
44 *Pseudomonas putida*, and *Bacillus subtilis* for *n*-butanol production⁸⁻¹¹. However, most of these
45 organisms are chemoheterotrophs. Thus, the *n*-butanol production using these microbes is also
46 carbon-positive.

47 To date, only a handful of studies have produced *n*-butanol autotrophically using CO₂ as a
48 carbon source¹²⁻¹⁶. Using a microbial electrosynthesis approach, a chemoautotroph *Clostridium*
49 sp. produced 135 mg/L of *n*-butanol at an applied potential (E_{appl}) of 0.8 V using CO₂ in 35 days¹².
50 This prolonged period was required for acid accumulation for *n*-butanol production using
51 *Clostridium* sp.⁷. Autotrophic *n*-butanol production was also demonstrated by an oxygenic
52 photoautotroph *Synechococcus elongatus* PCC 7942 using water as an electron donor¹⁴ and
53 sunlight as the energy source. Because, the *n*-butanol was generated using solar energy, this
54 product is called a solar fuel. With the *n*-butanol biosynthesis pathway, *S. elongatus* produced 2.2
55 mg/L *n*-butanol¹⁴ when incubated anaerobically under illumination. In contrast, aerobic incubation

56 did not generate any *n*-butanol. Furthermore, a dark anaerobic incubation of dense cultures (where
57 cells were not actively growing or evolving oxygen) produced 14 mg/L of *n*-butanol¹⁴. These
58 results suggest that oxygen (O₂) is detrimental to *n*-butanol production¹⁴. The ability of
59 cyanobacteria to produce *n*-butanol was later improved by several modifications such as 1) using
60 cofactor as a driving force¹⁵; 2) replacing the oxygen-sensitive enzyme involved in the *n*-butanol
61 producing pathway¹⁶, and 3) using intensive engineering to optimize the pathway in a multi-level
62 modular manner¹⁷. These engineered cyanobacterial strains produced 29.9 mg/L¹⁵, 404 mg/L¹⁶,
63 and 4.8 g/L¹⁷ of *n*-butanol. However, the low (<3%) energy conversion efficiency of natural
64 photosynthesis¹⁸ makes the use of cyanobacteria not ideal for *n*-butanol production.

65 To enhance energy conversion efficiency for biofuel production, artificial photosynthesis,
66 where photo-generated electrons were used to drive chemical reactions¹⁹, was developed. However,
67 due to catalyst limitations, hydrogen (H₂) was the main product²⁰. Although H₂ can be used as a
68 fuel, using such an explosive gas requires significant modifications to the current gasoline-based
69 infrastructures^{21,22}. To avoid this, a H₂-consuming chemoautotrophic bacterium *Ralstonia*
70 *eutropha*, was used for producing carbon-based liquid fuels using hybrid water-splitting
71 biosynthetic system. In this system, H₂ and O₂ were produced from water splitting (powered by
72 electricity from a potentiostat) using a cobalt phosphorus catalyst with an applied electrical
73 potential (E_{appl}) of 2.0 V¹⁹. The H₂ was then fed to the engineered *R. eutropha* to synthesize C₃-C₅
74 alcohol or polyhydroxybutyrate (PHB) from CO₂¹⁹. This hybrid biosynthetic system reached an
75 electrical energy conversion efficiency (EECE) up to ~20% using air (400 ppm CO₂) toward
76 biomass¹⁹. These values far exceeded the energy conversion efficiency of natural photosynthesis
77 Also, the system reported an EECE of 16 ± 2% towards C₄~C₅ alcohol using pure CO₂. Coupling
78 a solar panel/photovoltaic cell resulted in an energy conversion efficiency of 6% towards biomass

79 with pure CO₂²³. Although these studies provided a platform for indirect solar production from
80 CO₂, this technology is not an efficient and economical method for biofuel synthesis because, 1)
81 it produces O₂, which is detrimental to many biofuel synthesis processes¹⁴; 2) it uses H₂ as an
82 electron donor, which due to its low solubility limits electron transfer efficiency²⁴ and, finally; 3)
83 this system requires electrical potentials higher than 1.23 V¹⁸, making it an expensive method.
84 Therefore, it is critical to look for organisms that can overcome these limitations to advance
85 carbon-neutral biofuel production.

86 One such organism is the anoxygenic photoautotroph *Rhodospseudomonas palustris* TIE-1
87 (TIE-1). TIE-1 can use various carbon sources, such as atmospheric CO₂ and organic acids that
88 can be easily obtained from organic wastes²⁵. TIE-1 can also fix dinitrogen gas (N₂)²⁶, and use a
89 wide range of electron sources. These include H₂, which is a byproduct of many industries; ferrous
90 iron [Fe(II)], which is a naturally abundant element^{27,28}; and most importantly, poised electrodes
91 (i.e., photoelectroautotrophy) for its photosynthetic growth^{27,29-32}. This wide electron donor
92 selection enables TIE-1 to perform photosynthesis while avoiding O₂ generation, a harmful
93 component for biofuel synthesis¹⁴. TIE-1's ability to perform photoelectroautotrophy is
94 advantageous for biofuel production because of the direct electron uptake by TIE-1 from a poised
95 electrode bypasses the need for an indirect electron donor such as H₂. TIE-1 has a low E_{appl} (0.1
96 V)^{27,29-32} requirement, which lowers cost and electrochemical O₂ generation. TIE-1's E_{appl}
97 requirement is ~90% lower than that needed for water-splitting¹⁹, allowing us to use low-cost solar
98 panels to build novel biohybrid systems for solar fuel synthesis. Overall, TIE-1 is a superlative
99 biocatalyst that allows us to use extant CO₂, N₂, solar energy, and electrons generated by renewable
100 electricity for bioproduction. This process enables excess electricity to be stored as a usable fuel
101 or products for later use.

102 In a previous study *R. palustris* CGA009 (CGA009), a strain closely related to TIE-1, was
103 engineered to produce *n*-butanol from *n*-butyrate³³. In this study, the gene encoding the
104 alcohol/aldehyde dehydrogenases (AdhE2) from *R. palustris* Bisb18 was codon-optimized and
105 introduced into *R. palustris* CGA009³³. When cultured in the absence of CO₂, the modified
106 CGA009 was forced to reduce *n*-butyrate into *n*-butanol to maintain the redox balance³³. Although
107 this study used a phototroph that is closely related to TIE-1 for *n*-butanol production, this approach
108 is carbon-positive as it uses an organic substrate (*n*-butyrate).

109 To produce *n*-butanol in a sustainable and carbon-neutral manner, we introduced an
110 efficient, codon-optimized *n*-butanol biosynthesis pathway into TIE-1. This pathway, was
111 assembled using irreversible and efficient enzymes and produced 4.6 g/L *n*-butanol in *E. coli*³⁴.
112 The pathway contains five genes (*phaA*, *phaB*, *phaJ*, *ter*, *adhE2*)²⁷. Because TIE-1 possesses
113 homologs for the first two genes (*phaA* and *phaB*)²⁷, we designed two different cassettes (Fig. 1b),
114 containing either the whole (5-gene cassette) or a partial *n*-butanol biosynthesis pathway (3-gene
115 cassette). As shown in Fig. 1a, carbon (acetyl-CoA), and reducing equivalents (NADH) are two
116 major substrates for *n*-butanol biosynthesis. Previous studies in cyanobacteria have shown that a
117 PHB synthase deletion mutant produces higher butanol³⁵, and a glycogen synthase deletion mutant
118 showed higher carbon conversion efficiency (CCE) towards iso-butanol³⁶. We, therefore,
119 constructed TIE-1 knockout mutants lacking hydroxybutyrate polymerase¹⁸ or glycogen
120 synthase³⁷. Previous studies suggested that nitrogenase deletion mutants possess a more reduced
121 intracellular environment in *Rhodobacter capsulatus* and CGA009³⁷⁻³⁹. We predicted this would
122 be true in TIE-1 and created a nitrogenase double mutant. After introducing the 3-gene cassette/5-
123 gene cassette into the TIE-1 wild type (WT) and mutant strains, we tested *n*-butanol production
124 under both photoheterotrophic (Fig. 1c) and photoautotrophic (Fig. 1d) conditions. Under

125 photoelectroautotrophy, we used a novel hybrid bioelectrochemical cell (BEC) platform powered
126 by electricity from either an electrical grid powered potentiostat or a solar panel.

127 Our results show that the anoxygenic phototroph TIE-1 can produce *n*-butanol sustainably
128 using organic acids or CO₂ as carbon source, light as an energy source, and H₂, Fe(II), or electrons
129 from renewably generated electricity as an electron source. To the best of our knowledge, this
130 study represents the first attempt for biofuel production using a solar panel powered microbial
131 electrosynthesis platform, where CO₂ is directly converted to liquid fuel. Overall, these results
132 show that TIE-1 can be an attractive future microbial chassis for producing carbon-neutral biofuels
133 via synthetic biology and metabolic engineering, building upon our work using WT TIE-1 for
134 bioplastic production²⁷.

135

136 **Results**

137 **Deleting an electron-consuming pathway enhances *n*-butanol production**

138 We measured *n*-butanol production by WT with 3-gene cassette (WT+3), WT with 5-gene cassette
139 (WT+5), and TIE-1 mutants with either 3-gene (Nif+3, Gly+3, Phb+3) or 5-gene cassette (Nif+5,
140 Gly+5), under several photoheterotrophic and photoautotrophic conditions (substrate
141 combinations, incubation time and final optical density listed in Supplementary Table 1-1, 1-2
142 and 1-3) to identify the most productive strains and conditions.

143 For photoheterotrophic conditions, we chose acetate (Ac) or 3-hydroxybutyrate (3Hy) as
144 carbon and electron source because both substrates enter the *n*-butanol biosynthesis pathway
145 directly as their CoA derivatives (Supplementary Fig. 1)⁴⁰. For photoautotrophic conditions, we
146 used either H₂ or Fe(II) as an electron donor. CO₂ was supplied in all conditions to maintain the

147 pH of the medium and for redox balance in the cell. We provided N₂ or ammonia (NH₄⁺) as the
148 nitrogen source.

149 We found that depending on the carbon and electron source used, the same construct
150 produced variable amounts of *n*-butanol. *n*-Butanol production was the highest in the presence of
151 3Hy, followed by H₂, Ac, and Fe(II) (Fig. 2, Supplementary Table 2-1 and 2-2). We found that
152 Nif+5 is the most efficient *n*-butanol producer with highest production of 4.98 ± 0.87 mg/L under
153 the photoheterotrophic conditions with NH₄⁺ (Fig. 2b, Supplementary Table 2-1). The same
154 construct, however, produced ~10-fold lower *n*-butanol when incubated with Fe(II) (0.55 ± 0.03
155 mg/L) (Fig. 2d, Supplementary Table 2-1 and 2-2).

156 Compared to WT+3/WT+5, Nif+3/Nif+5 produced similar or more *n*-butanol depending
157 on the substrates, whereas Gly+3/Gly+5 and Phb+3 produced less *n*-butanol from all substrates
158 (Fig. 2, Supplementary Table 2-3). The presence of NH₄⁺ in the media has been reported to repress
159 the nitrogenase genes⁴¹. Therefore, we speculated that in its presence, WT+3/WT+5, and
160 Nif+3/Nif+5 would produce similar amounts of *n*-butanol. Surprisingly, in most cases,
161 Nif+3/Nif+5 produced a higher amount of *n*-butanol than the WT+3/WT+5, even in the presence
162 of NH₄⁺ (Fig. 2, Supplementary Table 2-3). Overall, we observe that deleting an electron-
163 consuming pathway (Nif) is beneficial, whereas deleting an acetyl-CoA-consuming pathway (Gly
164 and Phb) is detrimental to *n*-butanol production.

165 No *n*-butanol was detected from WT (no cassette added) using 3Hy as a carbon source. To
166 ensure the *n*-butanol production is not toxic to TIE-1⁷, we performed a toxicity assay. The lowest
167 inhibitory concentration of *n*-butanol for TIE-1 is 4050 mg/L (Supplementary Table 3-1), which
168 is much higher than the highest *n*-butanol production (4.98 ± 0.87 mg/L). Hence, the *n*-butanol
169 produced during our study does not limit the growth of TIE-1.

170

171 **Deleting acetyl-CoA-consuming pathways diverts carbon to acetone production**

172 Acetone is a major byproduct of *n*-butanol biosynthesis⁴⁰. As shown in Fig. 1a and Supplementary
173 Fig. 1, the accumulation of acetoacetyl-CoA, an intermediate in *n*-butanol biosynthesis, leads to
174 acetone production^{7,40}. We observed highest acetone production by Phb+3 (0.00 to 290.01 ± 47.51
175 mg/L) followed by Gly+3/Gly+5 (1.47 ± 0.08 mg/L to 192.84 ± 4.82 mg/L), WT+3/WT+5 (0.00
176 mg/L to 107.39 ± 3.74 mg/L), and Nif+3/Nif+5 (0.00 mg/L to 76.44 ± 1.12 mg/L) (Fig. 3
177 Supplementary Table 2-4). This acetone production trend is in the reverse order of *n*-butanol
178 production, i.e., Nif+3/Nif+5 produced the highest, and the Phb+3 produced the lowest amount of
179 *n*-butanol (Fig. 2, Supplementary Table 2-3). These results indicate that acetone biosynthesis likely
180 competes for acetyl-CoA with *n*-butanol biosynthesis. Using either Phb or Gly, acetyl-CoA that
181 would have otherwise been directed toward PHB or glycogen synthesis was diverted to acetone
182 biosynthesis.

183 Compared to using Ac as a substrate, which produced 0.00 mg/L to 37.29 ± 3.40 mg/L of
184 acetone, all constructs produced ~10-100-fold more acetone when supplied with 3Hy (18.15 ± 1.41
185 to 290.10 ± 38.80 mg/L (Fig. 3a, 3b, Supplementary Table 2-5, 2-6). However, when the same
186 strain was used, the acetone production under photoautotrophic conditions was lowered by ~25-
187 125-fold compared to photoheterotrophic conditions with only 0.00 to 3.92 ± 0.44 mg/L (Fig. 3c,
188 3d) (Supplementary Table 2-5, 2-6). These results indicate that under photoheterotrophic
189 conditions, particularly with 3Hy, TIE-1 accumulates more acetyl-CoA, which is eventually
190 converted into acetone. The high acetone production suggests that acetyl-CoA is not limiting for
191 *n*-butanol production. We also tested acetone toxicity in TIE-1 and found that the amount of
192 acetone produced does not limit TIE-1's growth (Fig. 3, Supplementary Table 3-2).

193
194
195
196
197
198
199
200
201
202
203
204
205
206
207
208
209
210
211
212
213
214
215

More reducing equivalents enhance carbon conversion efficiency (CCE) to *n*-butanol

To further identify the most efficient strain and substrate for *n*-butanol production with respect to carbon, we determined carbon consumption (Supplementary Fig. 2) and CCE for each construct under all conditions.

Carbon consumption - We have recently shown that TIE-1 can fix CO₂ during photoheterotrophic growth^{30,41}. Therefore, we also calculated CO₂ consumption and generation by all constructs. Under photoheterotrophy, all TIE-1 constructs consumed more (or generated less, represented by smaller negative value) CO₂ with 3Hy (up to -114.23 ± 4.52 to 78.67 ± 15.86 μmol) than Ac (up to -243.67 ± 5.79 to 53.79 ± 9.77 μmol) (Fig. 4a, 4b, Supplementary Table 2-7, 2-8). With either 3Hy or Ac, Nif+3/Nif+5 consumed more CO₂ (or generated less) CO₂ generation (-50.53 ± 8.01 to 78.67 ± 15.86 μmol) (Fig. 4a, 4b, Supplementary Table 2-9). These results are consistent with a previous study where the use of a more reduced substrate (such as 3Hy) resulted in more carbon consumption than the use of a more oxidized substrate (such as acetate) for redox balance⁴¹.

Similarly, under photoautotrophic conditions, Nif+3/Nif+5 consumed the highest amount CO₂ (36.41 ± 2.17 to 273.76 ± 27.25 μmol), except for Nif+3 incubated with H₂ and NH₄⁺ (Fig. 4c, 4d, Supplementary Table 2-9). This observation is likely due to the higher CO₂-fixation required to achieve redox balance in the absence of N₂-fixation. Gly+3/Gly+5 consumed the lowest amount of CO₂ ranging from -234.67 ± 5.79 to 99.04 ± 15.32 μmol (Fig. 4c, 4d, Supplementary Table 2-9). Glycogen mutants have been reported to fix less CO₂ compared to WT in cyanobacteria³⁶. This observation corroborates our result that Gly+3/Gly+5 produces low *n*-butanol under photoautotrophic conditions (Fig. 2c, 2d, Supplementary Table 2-3).

216 CCE - Similar to the trend for *n*-butanol production (Fig. 2), Nif+3/Nif+5 showed the highest CCE
217 (0.12 ± 0.03 to $4.58 \pm 0.23\%$), followed by WT+3/WT+5 (0.03 ± 0.01 to $1.70 \pm 0.32\%$),
218 Gly+3/Gly+5 (0.00 to $0.59 \pm 0.10\%$), and Phb+3 (0.00 to $0.16 \pm 0.04\%$) (Fig. 4, e-h Supplementary
219 Table 2-10). These results suggest that excess reducing equivalents enhanced *n*-butanol production
220 and facilitated CCE to *n*-butanol. In contrast, lack of the PHB or glycogen biosynthesis decreased
221 overall CCE to *n*-butanol. We found that all strains had the highest CCE when incubated with H₂
222 (0.00 to $4.58 \pm 0.23\%$), except for Phb (Fig. 4g, Supplementary Table 2-11, 2-12), which was
223 unable to produce *n*-butanol using any substrate (Fig. 2c). This high CCE in the presence of H₂
224 (Fig. 4g, Supplementary Table 2-11, 2-12) could be due to low acetone production (Fig. 3c,
225 Supplementary Table 2-5, 2-6) under this condition.

226 Higher CCE (1- to 7-fold) was observed when Nif+3/Nif+5 was supplied with N₂ compared
227 to NH₄⁺. For example, in the presence of NH₄⁺, Nif+3/Nif+5 showed CCE of 0.14 ± 0.01 to 1.61
228 $\pm 0.27\%$, which increased to 0.23 ± 0.01 to $4.58 \pm 0.23\%$ when N₂ was provided (Fig. 4 e-h,
229 Supplementary Table 2-13). In summary, excess reducing equivalents in the Nif mutant leads to
230 higher CCE towards *n*-butanol by TIE-1.

231

232 **More reducing equivalents enhance electron conversion efficiency to *n*-butanol**

233 To further identify the most productive strain and substrate toward *n*-butanol production with
234 respect to electron availability, we calculated each construct's electron conversion efficiency
235 (electron donor consumption data shown in Supplementary Fig. 2). We found that
236 photoautotrophic conditions are more favorable for higher electron conversion efficiency than the
237 photoheterotrophic conditions. With an electron conversion efficiency of 0.00 to $12.47 \pm 1.37\%$,
238 Fe(II) was the most efficient condition followed by H₂ (0.00 to $0.59 \pm 0.14\%$), Ac (0.00 to $0.49 \pm$

239 0.06 %), and 3Hy (0.00 to $0.07 \pm 0.01\%$) (Fig. 5, Supplementary Table 2-14, 2-15). The highest
240 electron conversion efficiency was observed in the presence of Fe(II)²⁷.

241 Using the same carbon and electron source, the highest electron conversion efficiency was
242 achieved by Nif+3/Nif+5 (0.04 ± 0.01 to $12.47 \pm 1.37\%$), followed by WT+3/WT+5 (0.00 to 6.45
243 $\pm 1.73\%$), Gly+3/Gly+5 (0.00 to $0.05 \pm 0.00\%$), and Phb+3 (0.00 to $0.03 \pm 0.01\%$, Fig. 5,
244 Supplementary Table 2-16). In summary, availability of reducing equivalents due to deletion of an
245 electron consuming pathway (Nif) leads to higher electron conversion efficiency for *n*-butanol
246 biosynthesis in TIE-1.

247

248 ***n*-Butanol bioproduction can be achieved with light, electricity, and CO₂**

249 We have recently demonstrated that the photoelectroautotrophic growth of TIE-1 leads to a highly
250 reduced intracellular environment compared to other growth conditions³⁰. Our data show that
251 excess reducing equivalents enhance *n*-butanol production in TIE-1. We further investigated *n*-
252 butanol production by TIE-1 under photoelectroautotrophy using a three-electrode sealed BEC
253 (Fig. 6a). We used Nif+5 in all BEC experiments as it was the most efficient *n*-butanol producer
254 under most of the tested conditions (Fig. 2c, 4c, 5g, Supplementary Table 2-3, 2-10, 2-16).

255 We created four distinct biofuel production BEC platforms by combining two different
256 electricity sources (grid-powered potentiostat or a solar panel) with two light sources (infrared or
257 halogen light). The potentiostat approach represents conventional electrical sources, while the
258 solar panel approach allows us to leverage renewably generated electricity. Infrared light is only a
259 small portion of the solar spectrum that specifically excites the photosystem of TIE-1²⁶. Halogen
260 light mimics natural sunlight that represents the solar spectrum^{42,43}. So, it can excite the
261 photosystem of TIE-1 and support electricity generation by a solar panel, simultaneously. *BEC*

262 *platform 1* used solar panel generated electrons and halogen light; *BEC platform 2* used solar panel
263 generated electrons and infrared light; *BEC platform 3* used potentiostat and halogen light; *BEC*
264 *platform 4* used potentiostat and infrared light. Either N₂ or NH₄⁺ was supplied as the nitrogen
265 source. Supplementary Table 1-4 lists detailed platform setups. We measured *n*-butanol production,
266 acetone production, and calculated CCE and electron conversion efficiency for each platform. We
267 also calculated the electrical energy conversion efficiency (EECE) by dividing the combustion
268 heat of the produced *n*-butanol by the electrical energy input.

269 The highest (0.91 ± 0.07 mg/L) and the lowest (0.19 ± 0.02 mg/L) *n*-butanol production
270 was achieved when N₂ was supplied as a nitrogen source in *BEC platform 1* and *BEC platform 2*,
271 respectively (Fig. 6b, Supplementary Table 2-17, 2-18). The BEC platforms powered by solar
272 panels showed 3-8 folds higher CO₂ consumption (Supplementary Fig. 3a, Supplementary Table
273 2-17) and 5-40 folds higher electron uptake (Supplementary Fig. 3b, Supplementary Table 2-
274 17)^{30,41} compared to the BEC platforms powered by the grid-powered potentiostat. Similar to the
275 other autotrophic conditions (Fig. 3c, 3d), little or no acetone was produced (Fig. 6c) from the
276 BEC platforms. BEC platform 4 achieved highest CCE ($0.49 \pm 0.06\%$, Fig. 6d, Supplementary
277 Table 2-17, 2-18) compared to the other three BEC platforms. Although BEC platforms powered
278 by grid powered potentiostat achieved much lower electron uptake (Supplementary Fig. 3b), they
279 reached a much higher electron conversion efficiency (6-25 folds) than the platforms powered by
280 a solar panel (Fig. 6e, Supplementary Table 2-17). This difference might be due to higher electrical
281 loss associated with the solar panel.

282 BEC platforms under halogen light achieved higher electron conversion efficiency (4 to 8-
283 fold, except using solar panel incubated with NH₄⁺, Fig. 6e, Supplementary Table 2-18) compared
284 to the BEC platforms using infrared light. However, the BEC platforms illuminated by halogen

285 light (platforms 1 and 3) had much lower (20-90%) electron uptake, particularly when using solar
286 panel as electricity source (Supplementary Fig. 3b Supplementary Table 2-18). To ensure that a
287 lower number of attached cells did not reduce electron uptake from the platforms using halogen
288 light, we performed live-dead viability assay. We observed that the percentage and number of live
289 cells attached to the electrodes were similar in all the BEC platforms (40%-50%) (Supplementary
290 Fig. 3c, and 3d, Supplementary Table 2-18). These results indicate that halogen light is not the
291 ideal light source for TIE-1 with respect to electron uptake.

292 We further compared the EECE between the two electricity sources. We found that the
293 BEC platforms powered by solar panel show lower EECE (1.62 ± 0.20 to $9.55 \pm 0.34\%$) than the
294 BEC platforms using a potentiostat (16.62 ± 1.01 to $131.13 \pm 3.97\%$) when the same nitrogen
295 source (either N_2 or NH_4) was supplied (Fig. 6f, Supplementary Table 2-17). With respect to the
296 light source, platforms using halogen light resulted in higher EECE (4.80 ± 0.38 to $131.14 \pm 3.97\%$)
297 than platforms using infrared light (1.62 ± 0.20 to $26.52 \pm 2.87\%$) when the same nitrogen source
298 was supplied (6f, Supplementary Table 2-18). Halogen light represents the solar spectrum and
299 several wavelengths from this light source can be absorbed by TIE-1 via the light-harvesting
300 complexes and eventually, the photosystem^{30,44}. This would lead to higher ATP synthesis via
301 cyclic photosynthesis by TIE-1³⁰ perhaps explaining the greater than 100% EECE.

302 In summary, *BEC platform 1* showed higher *n*-butanol production, *BEC platform 4* showed
303 the highest CCE, and *BEC platform 3* showed the highest electron conversion efficiency and EECE.
304 Although *BEC platform 1* resulted in moderate conversion efficiencies, the highest *n*-butanol
305 production (up to 5-fold) with the use of sustainable resources (electricity from solar panel and
306 energy from halogen light), make this platform the most promising for further development as a
307 sustainable and carbon-neutral process for *n*-butanol production.

308

309 **Discussion**

310 In recent years, *n*-butanol has been proposed as a superior biofuel due to its higher energy content,
311 lower volatility, and reduced hydrophilicity⁴. Here we produced *n*-butanol by introducing an
312 artificial *n*-butanol biosynthesis pathway³⁴ into an anoxygenic photoautotroph *Rhodospseudomonas*
313 *palustris* TIE-1²⁶. Using metabolic engineering and novel hybrid bioelectrochemical platforms, we
314 show that TIE-1 can produce *n*-butanol using different carbon sources (organic acids, CO₂),
315 electron sources [H₂, Fe(II), a poised electrode], and nitrogen sources (NH₄⁺, N₂). TIE-1's ability
316 to produce *n*-butanol under photoelectroautotrophy using light, electricity, and CO₂ can serve as a
317 stepping-stone for sustainable solar fuel production.

318 After introducing a codon-optimized *n*-butanol biosynthesis pathway in TIE-1 and its
319 mutants (Nif, Gly, and Phb), we determined *n*-butanol production, acetone production, CCE, and
320 electron conversion efficiency of these constructs under both photoheterotrophic and
321 photoautotrophic conditions. Mutants lacking the nitrogen-fixing pathway (Nif+3/Nif+5) (known
322 to affect redox balance in the cell by consuming reducing equivalents^{37,39,45}) exhibited a more
323 reduced intracellular environment (indicated by higher CO₂ fixation)⁴¹ and produced more *n*-
324 butanol compared to WT+3/WT+5. In contrast, deleting acetyl-CoA-consuming pathways
325 (Gly+3/Gly+5 and Phb+3) led to lower *n*-butanol production. These results show that higher
326 reducing equivalent rather than increased acetyl-CoA availability enhances *n*-butanol production
327 by TIE-1. These results also agree with previous works where redox balance or reducing equivalent
328 availability plays a vital role in *n*-butanol production^{33,46}. A closely related strain *R. palustris*
329 CGA009 has been shown to produce *n*-butanol when its biosynthesis was the obligate route for
330 maintaining redox balance during photoheterotrophic growth on *n*-butyrate³³. Similarly, in *E. coli*,

331 *n*-butanol production increased when its biosynthesis acted as an electron-sink to rescue cells from
332 redox imbalance⁴⁶.

333 We expected that the presence of NH₄⁺ would inhibit the expression of nitrogenase, so
334 nitrogen fixation would not occur. Thus, nitrogenase would not produce the byproduct H₂^{45,47,48}.
335 However, we observed that WT+3/WT+5 and Gly+3/Gly+5 produced H₂ (likely via nitrogenase)
336 despite the presence of NH₄⁺ (Supplementary Fig. 2). This was in contrast to the Nif+3/Nif+5,
337 which did not produce H₂ under any condition, confirming that the observed H₂ production in the
338 WT and Gly strains is due to nitrogenase activity. The production of H₂ by nitrogenase is well
339 known in CGA009^{38,39,41}. This unexpected nitrogenase activity could have been initiated by the
340 lower NH₄⁺ concentrations toward the end of the experiment, which might lead to the induction of
341 nitrogenase gene expression^{47,49}. Because H₂ production via nitrogenase even in the presence of
342 NH₄⁺ consumes reducing equivalents, this explains why the Nif strains produce more *n*-butanol
343 compared to the WT and Gly strains.

344 We also observed that by feeding *n*-butanol biosynthesis pathway intermediates as a carbon
345 source, such as 3Hy, TIE-1 produced more *n*-butanol (Fig. 2). However, despite high *n*-butanol
346 production with 3Hy, TIE-1 showed low CCE and low electron conversion efficiency, possibly
347 due to higher acetone production (Fig. 3). This high acetone production is likely due to the
348 accumulation of acetoacetyl-CoA, converted from 3Hy through 3-hydroxybutyryl-CoA
349 (Supplementary Fig. 1)⁵⁰. This along with 3Hy being an expensive feedstock compared to CO₂ for
350 bioproduction^{51,52} makes it an unsuitable substrate for economical *n*-butanol production.

351 In general, we achieved higher *n*-butanol production, CCE, and electron conversion
352 efficiency when acetone production was lower. These results agree with the previous studies where
353 an increase in *n*-butanol production accompanies a decrease in acetone production^{53,54}. Although

354 using highly reduced substrates, such as glycerol, can increase the ratio of *n*-butanol to acetone, a
355 significant amount of acetone is always detected while using the *n*-butanol biosynthesis pathway
356 from *C. acetobutylicum*^{53,54}. Our study addressed this issue by using slow or non-growing cells
357 that produced *n*-butanol without the production of acetone.

358 BEC platforms powered by the potentiostat resulted in higher EECE and electron
359 conversion efficiency. This difference might be due to either electrical or optical losses associated
360 with the solar panel during photoelectron generation^{55,56}. The electrical loss could be due to the
361 limited energy efficiency of the solar panel, which is determined by the diode characteristics and
362 series resistances in the solar panel^{55,56}. And optical loss can be in the form of poor light absorbance
363 or light reflection from the solar cell surfaces or material defects^{57,58}. We found that the platforms
364 with halogen as the light source have higher EECE (~8 fold) regardless of the electricity source.

365 To contextualize our results, we compared EECE, E_{appl} , and *n*-butanol production, and CCE
366 with the previous related studies.

367 *EECE* – Using solar panel generated electricity TIE-1 achieved an EECE of up to 9.54%, which
368 increased by over 13-fold (up to 131.13%) when we used grid-based electricity (Fig. 6f). In a
369 previous study using a hybrid water-splitting system, *R. eutropha* achieved an EECE of 16%
370 towards C₄+C₅ alcohol using grid-based electricity¹⁹. These data suggest that TIE-1 can achieve
371 higher EECE.

372 *E_{appl} and power requirement* – TIE-1 can gain electrons directly from an electrode, which requires
373 lower E_{appl} for photoautotrophic growth and *n*-butanol biosynthesis ($E_{\text{appl}} = 0.1 - 0.5$ V). In contrast,
374 the hybrid water splitting system used to synthesize C₃-C₅ alcohol or PHB by *R. eutropha* used an
375 E_{appl} of 2.0 V. Similarly, *n*-butanol synthesis by *Clostridium* sp. using MES used an E_{appl} of 0.8
376 V^{12,19}. Assuming that all the reactors use 1 mA of current, the power would be 5×10^{-4} W for *n*-

377 butanol bioproduction by TIE-1. In contrast, *R. eutropha* would require 2×10^{-3} W for water-
378 splitting, and *Clostridium* sp. would require 8×10^{-4} W. Therefore, TIE-1 uses four times less
379 power than *R. eutropha* and 1.6 times less power than *Clostridium* sp. This implies that even low-
380 efficiency solar panel-based platforms⁵⁷, and low sunlight conditions can more be easily used for
381 bioproduction using organisms like TIE-1^{59,60}.

382 *n-Butanol production* – Under photoelectroautotrophy, TIE-1 produced 0.91 ± 0.07 mg/L of *n*-
383 butanol in 10 days (Fig. 6b). *Clostridium* sp. produced 135 mg/L *n*-butanol in 35 days¹². Compared
384 to *R. eutropha* and *Clostridium* sp., our platform produced lower *n*-butanol. Under
385 photoautotrophic conditions, TIE-1 produced a maximum of 3.09 ± 0.25 mg/L of *n*-butanol in
386 batch culture (Fig. 2c). Initial studies in cyanobacteria resulted in 2.2 mg/L¹⁴. Recently, using a
387 modular engineering method, cyanobacteria can produce 4.8 g/L of *n*-butanol¹⁷, which is 2000
388 times higher than the initial production. With intensive future engineering efforts, we anticipate
389 that TIE-1 can also demonstrate higher *n*-butanol production.

390 *CCE* – To the best of our knowledge, no autotrophic *n*-butanol production study has reported CO₂
391 consumption^{14-17,35,36}. Thus, here we compared TIE-1's CCE with that reported for heterotrophic
392 *n*-butanol production. Although most heterotrophic growth media use yeast extract (an undefined
393 carbon source), for simplicity, the CCE calculations considered glucose as the only carbon source.
394 We calculated CCE using the total amount of added carbon in these studies^{9,61}. Considering the
395 additional contribution of yeast extract would lower the CCE further. The early trials in *E. coli* and
396 *S. cerevisiae* reached carbon conversion efficiencies of 0.11 % and 0.02%. With intensive
397 metabolic engineering, the CCE reached 45.92% (*E. coli*) and 11.52% (*S. cerevisiae*) (calculated
398 from the reported g/g yield)^{34,62}. In this initial study here, we show that TIE-1 shows CCE (mol/mol)
399 of $4.58 \pm 0.21\%$ and $1.95 \pm 0.26\%$ under photoautotrophic and photoheterotrophic conditions,

400 respectively (Fig. 4). This is 20 and 200 times higher than that of initial studies in *E. coli* and *S.*
401 *cerevisiae*. Photoautotrophic bioproduction is superior due to the low cost of CO₂ compared to
402 heterotrophic substrates⁵². Thus, developing TIE-1 further via metabolic engineering, synthetic
403 biology, and bioprocess engineering will make it an economically viable bioproduction platform.

404 In summary, TIE-1 can achieve high electrical energy conversion efficiency, and CCE
405 with lower power input, while producing an amount of *n*-butanol comparable to the initial studies
406 in established bioproduction chassis organisms like *E. coli*, and *S. cerevisiae*. This study represents
407 the initial effort of producing carbon-neutral fuels using TIE-1. Countless modifications could be
408 made to improve the *n*-butanol titer. For example, we observed an increased expression of genes
409 in the *n*-butanol biosynthesis pathway from Nif+5 incubated with 3Hy (the strain and condition
410 that resulted in the highest *n*-butanol production) (Supplementary Fig. 4). Therefore, increasing
411 gene expression by driving each gene in the *n*-butanol biosynthesis pathway with its own promoter
412 could increase *n*-butanol production. Also, since reducing equivalent availability seems to be a
413 bottleneck for *n*-butanol production, deleting more pathways that consume electrons could
414 increase *n*-butanol production. Also, increasing intracellular iron could lead to higher cytochrome
415 production, which would increase electron uptake⁶³. Furthermore, creating a BEC platform with
416 built-in solar conversion to electricity capability could reduce electrical energy loss. Finally, higher
417 electron uptake, which should be beneficial for *n*-butanol synthesis, could be achieved by using
418 nanoparticle modified electrodes^{31,64,65}. Taken together, TIE-1 offers a sustainable route for
419 carbon-neutral *n*-butanol biosynthesis and other value-added products. As CO₂ concentrations are
420 rising in the atmosphere, such bioproduction strategies need immediate attention and support.

421

422 **Materials and Methods**

423 **Bacterial strains, media, and growth conditions**

424 All strains used in this study are listed in Supplementary Table 1-5. *E. coli* strains were grown in
425 lysogeny broth (LB; pH 7.0) at 37°C. For aerobic growth, *Rhodospseudomonas palustris* TIE-1 was
426 grown at 30 °C in YP medium (3 g/L yeast extract, 3 g/L peptone) supplemented with 10 mM
427 MOPS [3-N (morpholino) propanesulphonic acid] (pH 7.0) and 10 mM succinate (YPSMOPS) in
428 the dark. For growth on a solid medium, YPSMOPS or LB was supplemented with 15 g/L agar.
429 For anaerobic phototrophic growth, TIE-1 was grown in anoxic bicarbonate buffered freshwater
430 (FW) medium²⁷. All FW medium was prepared under a flow of 34.5 kPa N₂ + CO₂ (80%, 20%)
431 and dispensed into sterile anaerobic Balch tubes. The cultures were incubated at 30°C in an
432 environmental chamber fitted with an infrared LED (880 nm). For photoheterotrophic growth, the
433 FW medium was supplemented with 50 mM MOPS at pH 7.0 and sodium 3-hydroxybutyrate or
434 sodium acetate at pH 7.0, to a final concentration of 50 mM. For photoautotrophic growth on iron,
435 anoxic sterile stocks of FeCl₂ and nitrilotriacetic acid (NTA) were added to reach final
436 concentrations of 5 mM and 10 mM, respectively. For photoautotrophic growth on H₂, TIE-1 was
437 grown in FW medium at pH 7.0 and 12 psi of 80% H₂/20% CO₂²⁷. For all carbon and electron
438 sources, either ammonium chloride (5.61 mM) or dinitrogen gas (8 psi) was supplied as nitrogen
439 source²⁷. All sample manipulations were performed inside an anaerobic chamber with a mixed gas
440 environment of 5% H₂/75% N₂/20% CO₂. When needed, 400 µg/mL kanamycin was added for
441 TIE-1, and 50 µg/mL kanamycin was added for *E. coli*.

442

443 ***R. palustris* TIE-1 deletion mutant construction**

444 We constructed three mutants, two of which were double mutants using the method described in a
445 previous study³⁰. Respectively, Glycogen synthase knockout was created by deleting Rpal_0386,

446 nitrogenase knockout was created by deleting Rpal_1624, and Rpal_5113, and hydroxybutyrate
447 polymerase knockout was created by deleting and Rpal_2780 and Rpal_4722 were deleted
448 resulting hydroxybutyrate polymerase knockout. Briefly, the 1 kb upstream and 1 kb downstream
449 regions of the gene were PCR amplified from the *R. palustris* TIE-1 genome, then the two
450 homology arms of the same gene were cloned into pJQ200KS plasmid. The resulting vector was
451 then electroporated into *E. coli* and then conjugated to *R. palustris* TIE-1, using the mating strain
452 *E. coli* S17-1/λ. After two sequential homologous recombination events, mutants were screened
453 by PCR, as shown in Supplementary Fig. 5. The primers used for mutant construction and
454 verification are listed in Supplementary Table 1-6 and 1-7.

455

456 **Plasmid construction**

457 All plasmids used in this study are listed in Supplementary Table 1-8. There are five genes
458 involved in the *n*-butanol biosynthesis: *phaJ*, *ter*, *adhE2*, *phaA*, and *phaB* (Fig. 1a). Among these
459 five genes, TIE-1 has homologs of the first two (*phaA* and *phaB*). Hence, we designed two different
460 cassettes, namely, a 3-gene cassette (3-gene), which has *phaJ*, *ter*, *adhE2*, and a 5-gene cassette
461 (5-gene), which has the 3-gene plus a copy of the *phaA-phaB* operon from TIE-1. *phaJ*, *ter*, and
462 *adhE2* sequences were obtained from published studies³⁴. The *phaJ* gene, isolated from
463 *Aeromonas caviae*, was chosen because it codes for an enzyme that has a higher specificity for its
464 substrate^{34,66}. The *ter* gene isolated from *Euflena gracilis* was selected because it is unable to
465 catalyze the reverse oxidation of butyryl-CoA³⁴. The *adhE2* gene isolated from *C. acetobutylicum*
466 chosen because the enzyme encodes for specifically catalyzes the reduction of the butyryl-CoA³⁴.
467 All three foreign genes (*phaJ*, *ter*, and *adhE2*) were codon-optimized by Integrated DNA
468 Technology (IDT) for TIE-1. The cassette was synthesized as G-blocks by IDT, which we then

469 stitched together by overlap extension and restriction cloning. The *phaJ-ter-adhE2* cassette was
470 then inserted into plasmid pRhokS-2, resulting in pAB675. *PhaA* and *phaB* were amplified as an
471 operon from the *R. palustris* TIE-1 genome. The *phaA-phaB* cassette was then cloned into pAB675
472 to obtain pAB744. Upon obtaining mutants and plasmids, either the 3-gene or the 5-gene was
473 conjugated into WT TIE-1 or the mutants, using mating the strain *E. coli* S17-1/ λ . All conjugations
474 were successful, except for the 5-gene into the $\Delta phaC1\Delta phaC2$. The primers used for cassette
475 construction are listed in Supplementary Table 1-9. The primers used for cassette sequencing are
476 listed in Supplementary Table 1-10.

477

478 **Substrate measurement**

479 Substrate concentrations at the beginning (T_0) and the end (T_f) were measured to calculate carbon
480 and electron conversion efficiency to *n*-butanol. The incubation time of each experiment can be
481 found in Supplementary Table 1-2.

482 **a) CO₂ and H₂ analysis by gas chromatography**

483 CO₂ and H₂ were analyzed using a method described in a previous study²⁷. Gas samples were
484 analyzed using gas chromatography (Shimadzu BID 2010-plus, equipped with Rt[®]-Silica BOND
485 PLOT Column, 30 m \times 0.32 mm; Restek, USA) with helium as a carrier gas. To measure the CO₂
486 content of the liquid phase, 1 mL of the cell-free liquid phase was added to 15 mL helium-flushed
487 septum-capped glass vials (Exetainer, Labco, Houston) containing 1 mL 85% phosphoric acid.
488 Then 40 μ L of the resulting gas from the Balch tube was injected into the Shimadzu GC-BID, using
489 a Hamilton[™] gas-tight syringe. To measure the CO₂ and H₂ contents of the gas phase, either 40
490 μ L of the gas phase was directly injected into the Shimadzu GC-BID, or 5 mL of the gas phase

491 was injected into a 15 mL helium-flushed septum-capped glass vial (Exetainer, Labco, Houston),
492 using a HamiltonTM gas-tight syringe. Then 50 μ L of the diluted gas sample was injected into the
493 Shimazu GC-BID, using a HamiltonTM gas-tight syringe. A standard curve was generated by the
494 injection of 10 μ L, 25 μ L, and 50 μ L of H₂ + CO₂ (80%, 20%). The total moles of CO₂ in the
495 reactors were calculated using the ideal gas law ($PV=nRT$)⁶⁷.

496 **b) Organic acid analysis by ion chromatography**

497 The acetate and 3-hydroxybutyrate concentrations were measured as described previously ²⁷.
498 Briefly, after 1:50 dilution, the acetate and 3-hydroxybutyrate concentrations at the starting and
499 endpoint of culture for each sample were quantified using an Ion Chromatography Metrohm 881
500 Compact Pro with a Metrosep organic acid column (250 mm length). Eluent (0.5 mM H₂SO₄ with
501 15% acetone) was used at a flow rate of 0.4 mL min⁻¹ with suppression (10 mM LiCl regenerant)²⁷.

502 **c) Ferrous iron [Fe(II)] analysis by ferrozine assay**

503 The Fe(II) concentration was measured using ferrozine assay, as described in a previous study²⁷.
504 Briefly, 10 μ L of culture was mixed with 90 μ L 1M HCl in a 96-well plate inside the anaerobic
505 chamber with 5% H₂/75% N₂/20% CO₂ (Coy laboratory, Grass Lake). After the plate was removed
506 from the anaerobic chamber, 100 μ L of ferrozine (0.1% (w/v) ferrozine in 50% ammonium acetate)
507 was added to the sample. Then the 96-well plate was covered with foil and incubated at room
508 temperature for 10 minutes before the absorbance was measured at 562 nm. The absorbance was
509 then converted to Fe(II) concentration based on a standard curve generated by measuring the
510 absorbance from 0 mM, 1 mM, 2.5 mM and, 5 mM Fe(II).

511

512 ***In vivo* production of *n*-butanol**

513 The plasmids with the *n*-butanol pathway were unstable when adapting the strain to the nitrogen-
514 fixing or photoautotrophic conditions. To avoid this problem, a twice-washed heavy inoculum
515 from YPSMOPS was used under all conditions. All strains were inoculated in 50 mL of YPSMOPS
516 with kanamycin with a 1:50 dilution from a pre-grown culture. When the OD₆₆₀ reached 0.6-0.8,
517 the culture was inoculated into 300 mL of YPSMOPS with kanamycin. When the OD₆₆₀ reached
518 0.8~1, 10 mL of culture was saved for a PCR check (Supplementary Fig. 6). The rest of the culture
519 was washed twice with ammonium-free FW medium and resuspended using anoxic ammonium
520 free FW medium inside the anaerobic chamber. Finally, the culture was inoculated into the
521 medium containing different carbon sources and electron donors (acetate, 3-hydroxybutyrate, H₂,
522 Fe(II), or electrode) in either a sealed Balch tube (initial OD₆₆₀ ~1) or a bioelectrochemical cell
523 (initial OD₆₆₀ ~0.7). The tubes and the reactors were sealed throughout the process, and samples
524 were taken after the cultures reached the stationary phase (incubation time listed in Supplementary
525 Table 4), using sterile syringes.

526

527 **Extraction and quantification of *n*-butanol and acetone**

528 After the culture entered the late stationary phase, 1 mL of culture was removed from the culture
529 tube using a syringe and centrifuged at 21,100X *g* for 3 minutes. The supernatant was then filtered
530 using a syringe filter, and the filtrate or the standard was extracted with an equal volume of toluene
531 (containing 8.1 mg/L iso-butanol as an internal standard) and mixed using a Digital Vortex Mixer
532 (Fisher) for 5 minutes, followed by centrifugation at 21,100X *g* for 5 minutes. After centrifugation,
533 250 µL of the organic layer was added to an autosampler vial with an insert. The organic layer was
534 then quantified with GC-MS (Shimadzu GCMS-QP2010 Ultra), using the Rxi[®]-1ms column. The
535 oven was held at 40 °C for 3 minutes, ramped to 165 °C at 20 °C/min, then held at 165 °C for 1

536 min. Samples were quantified relative to a standard curve for 0 mg/L, 0.2025 mg/L, 0.405 mg/L,
537 0.81 mg/L, 2.025 mg/L, 4.05 mg/L, and 8.1 mg/L of *n*-butanol and 0 mg/L, 0.784 mg/L, 3.92 mg/L,
538 7.84 mg/L, 39.2 mg/L, 78.4 mg/L, and 392 mg/L of acetone. An autosampler was used to reduce
539 the variance of injection volumes.

540

541 **Bioelectrochemical platforms and growth conditions**

542 A three-electrode sealed-type bioelectrochemical cell (BEC, C001 Seal Electrolytic Cell, Xi'an
543 Yima Opto-electrical Technology Com., Ltd, China)^{30,64} containing 80 mL of FW medium was
544 used for testing *n*-butanol production. The three electrodes were configured as a working electrode
545 (a graphite rod, 3.2 cm²), a reference electrode (Ag/AgCl in 3.5M KCl), and a counter electrode
546 (Pt foil, 5 cm²). FW medium (76 mL) was dispensed into sterile, sealed, three-electrode BECs,
547 which were bubbled for 60 minutes with N₂ + CO₂ (80%/20%) to remove oxygen and pressurized
548 to ~7 psi. Four BECs were operated simultaneously (*n*=3 biological replicates) with one no-cell
549 control. All photoelectroautotrophic experiments were performed at 26 °C under continuous
550 infrared light (880 nm) or halogen light. The electrical potential of 0.5 V ($E_{\text{appl}}=0.5$ V) was
551 constantly applied between the working electrode and counter electrode using a grid powered
552 potentiostat (Interface 1000E, Gamry Multichannel potentiostat, USA) or solar panel (Uxcell 0.5V
553 100mA Poly Mini Solar Cell Panel Module) for 240 hrs. Electron uptake and current density were
554 collected every 1 minute using the Gamry Echem Analyst™ (Gamry Instruments, Warmister, PA)
555 software package. At the end of the bioelectrochemical experiment, the samples were immediately
556 collected from the BEC reactors. *n*-butanol, acetone, and substrates were measured as described
557 above.

558

559 **Calculations of CCE, electron conversion efficiency, and electrical conversion efficiency**

560 CCE, electron conversion efficiency, and electrical energy conversion efficiency (EECE) were
561 calculated by dividing the total carbon/electrons/electrical-energy consumption by the final
562 carbon/electrons/energy content in *n*-butanol, respectively.

563 To determine carbon consumption, acetate, 3-hydroxybutyrate, or CO₂ consumption was
564 calculated by subtracting the amount in the sample at the end of the experiment from the amount
565 at the beginning of the experiment. Then all the carbon substrate consumptions were converted to
566 moles of carbon, using Equation 1. The amount of carbon converted to *n*-butanol was calculated
567 based on the *n*-butanol production, using Equation 2. The CCE was calculated using Equations 1,
568 2, and 3 below:

569
$$\text{C mol substrate} = \text{consumed substrate (mol / L)} * \text{mol of C in 1 mol substrate} \quad (1)$$

570
$$\text{C mol } n\text{-butanol} = \frac{n\text{-butanol (g / L)} * \text{mol of C in 1 mol } n\text{-butanol}}{\text{molecular weight of } n\text{-butanol}} \quad (2)$$

571

572
$$\text{Carbon conversion efficiency} = \frac{\text{C mol } n\text{-butanol}}{\text{C mol substrate}} * 100\% \quad (3)$$

573 The theoretical total number of electrons available from each consumed electron donor was
574 calculated as described below (Equation 4). The total available electrons from the complete
575 oxidation of each organic acid were calculated with the assumption that the final oxidation product
576 was CO₂. The inorganic electron donors such as Fe(II) and H₂ release 1 mole e⁻ and 2 moles e⁻ per
577 mole, respectively. Electrons supplied for the photoelectroautotrophy condition were calculated
578 directly from BEC based experiments wherein the total current uptake was integrated over the
579 operational time. The total electron uptake was used to calculate the electron conversion efficiency

580 to *n*-butanol because the electrode is the direct electron donor under this growth condition. The
581 number of electrons required for *n*-butanol production was calculated from the oxidation state of
582 the carbon in each carbon source and *n*-butanol. Supplementary Table 4 lists the specific oxidation
583 state, and the number of electrons required per mole of *n*-butanol is listed for all studied sources
584 and *n*-butanol.

585 To calculate total available electrons from each substrate, the amount of consumed
586 substrate (in moles) was multiplied by the theoretical total available electrons per mole of the
587 substrate when fully oxidized to CO₂ (Equation 4). For photoelectroautotrophy, the total available
588 electron was calculated based on data collected from a data acquisition system (DAQ, Picolog
589 Datalogger). To obtain the electrons required for *n*-butanol production, the *n*-butanol production
590 (in moles) was multiplied by the theoretical number of electrons required per mole (Equation 5).
591 The conversion efficiency was calculated by dividing the moles of electrons required for *n*-butanol
592 production by the theoretical total available electrons (Equation 6).

$$593 \quad e^{-} \text{ mol substrate} = \text{consumed substrate (mol)} * \text{total available electrons in the substrate} \quad (4)$$

$$594 \quad e^{-} \text{ mol } n\text{-butanol} = n\text{-butanol (mol)} * \text{electrons required to synthesize 1 mol } n\text{-butanol} \quad (5)$$

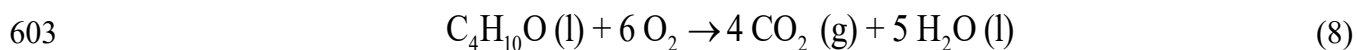
$$595 \quad \text{Electron conversion efficiency} = (e^{-} \text{ mol } n\text{-butanol}) / (e^{-} \text{ mol substrate}) * 100\% \quad (6)$$

596 Calculation of the electrical energy conversion efficiency (EECE) to *n*-butanol was adapted
597 from a previous study¹⁹. The EECE was calculated by equation 7. The charge supplied to the
598 bioelectrochemical platforms was calculated from data collected by DAQ.

$$599 \quad \text{EECE} = \frac{\Delta_r G^0 \text{ gain from CO}_2 \text{ to } n\text{-butanol}}{\text{charge passed through (C)} * \text{applied voltage (V)}} * 100\% \quad (7)$$

600

601 The Gibbs free energy gains ($\Delta_r G^0$) for *n*-butanol was calculated similarly with a previous
602 study¹⁹ by reaction 8 and equation 9⁶⁸.



$$604 \quad \Delta_r G^0_{(\text{C}_4\text{H}_{10}\text{O})} = \Delta_f H^0_{(\text{C}_4\text{H}_{10}\text{O})} - 5 * \Delta_f H^0_{(\text{H}_2\text{O})} - 4 * \Delta_f H^0_{(\text{CO}_2)} - 6 * \Delta_f H^0_{(\text{O}_2)} \quad (9)$$

$$605 \quad \Delta_f H^0_{(\text{C}_4\text{H}_{10}\text{O})} = -277.4 \text{ kJ/mol}, \Delta G^0_{(\text{CO}_2)} = -394.39 \text{ kJ/mol}, \Delta G^0_{(\text{H}_2\text{O})} = -273.14 \text{ kJ/mol}, \Delta G^0_{(\text{O}_2)} = 0 \text{ kJ/mol}$$

606

607 RNA extraction, cDNA synthesis, and RT-qPCR

608 To extract RNA for cDNA synthesis and eventually perform RT-qPCR for analyzing the
609 expression level of the individual genes, culture samples (2.5 ml to 15 ml depending on OD₆₆₀)
610 were taken at the late exponential (T_m) or stationary phase (T_f). Samples were immediately
611 stabilized with an equal volume of RNAlater (Qiagen, USA). After incubation at room temperature
612 for 10 min, samples were centrifuged at 21,100 *g for three minutes. After the supernatant was
613 removed, the pellet was stored at -80°C before RNA extraction using the Qiagen RNeasy Mini kit
614 (Qiagen, USA), following the manufacturer's protocol. DNA was removed using a Turbo DNA-
615 free Treatment and Removal Kit (Ambion, USA). DNA contamination was ruled out by PCR using
616 the primers listed in Supplementary Table 1-11.

617 Purified RNA samples were then used for cDNA synthesis by an iScript™ cDNA Synthesis
618 Kit (Biorad, USA). The same mass of RNA was added to each cDNA synthesis reaction. The
619 synthesized cDNA was used for RT-qPCR. RT-qPCR was performed using the Biorad CFX
620 connect Real-Time System Model # Optics Module A with the following thermal cycling
621 conditions: 95 °C for 3 min, then 30 three-step cycles of 95 °C for 3 seconds, 60 °C for 3 min, and
622 65 °C for 5 seconds, according to the manufacturer's manual. The reaction buffer was iTaq SYBR
623 Green Supermix with ROX (Bio-Rad). The primers used for RT-qPCR (listed in Supplementary

624 Table 1-11) were designed using primer3 software (<http://bioinfo.ut.ee/primer3/>). The primer
625 efficiencies were determined by performing RT-qPCR using different DNA template
626 concentrations. The genes *clpX* and *recA*, which have been previously validated as internal
627 standards, were used for the genome^{29,30}. The gene code for kanamycin resistance was also used
628 as an internal standard for the plasmid. After RT-qPCR, the data were analyzed using the C_T
629 method. Fold changes, and standard deviations were calculated as described in a previous study²⁷.

630

631 **Viability analysis of TIE-1 under photoelectroautotrophy.**

632 WT TIE-1 was inoculated into the bioelectrochemical reactors described above, with a starting
633 OD of ~0.3. After 72 hours of incubation, the viability of the biofilm of the electrode was
634 characterized by imaging the electrode stained with LIVE/DEAD[®] (L7012, Life Technologies),
635 and then the attached cells were quantified using NIS-Elements AR Analysis 5.11.01 64-bit
636 software. Imaging of the electrode was performed as described in a previous study³⁰. Prior to
637 cutting a piece of the spent electrode, the electrode from the reactor was washed 3 times with 1X
638 phosphate-buffered saline (PBS) to remove unattached cells. A piece of the spent electrode was
639 then submerged in 1X PBS in a sterile microfuge tube. Prior to imaging, the electrode piece was
640 immersed in LIVE/DEAD[®] stain (10 μ M SYTO9 and 60 μ M propidium iodide) kit and incubated
641 for 30 minutes in the dark. The electrode sample was then placed in a glass-bottom Petri dish
642 (MatTek Corporation, Ashland, MA) containing enough PBS to submerge the sample. Further, it
643 was imaged on a confocal microscope (Nikon A1 inverted confocal microscope), using 555 and
644 488 nm lasers and a 100X objective lens (Washington University in St. Louis Biology Department
645 Imaging Facility). Electrode attached cells were quantified by Elements Analysis software using
646 the protocol described below: Briefly, for each reactor, three images were processed. Z-stacks of

647 each image were split into two channels (one for live cells, one for dead cells), the MaxIP was
648 acquired for the combined z-stacks. After GaussLaplace, local contrast and smoothing, and
649 thresholding, and Object Count was performed for each channel based on a defined radius (0.8 μ m~
650 5 μ m). Then the percentage of live (or dead) cells was calculated by

$$651 \quad \text{Live (or Dead)cell percentage} = \frac{\text{number of Live (or Dead) cells}}{\text{number of total cells}} * 100\%$$

652 The viability of planktonic cells was determined by RT-qPCR of the essential genes (ATP synthase
653 homologs: *atp1*, *atp2*) and the genes involved in photoelectroautotrophy (photosynthetic reaction
654 center: *pufL*, ribulose-1,5-bisphosphate carboxylase/oxygenase: *ruBisCo1*, *ruBisCo2*, and *pio*
655 operon: *pioA*) (Supplementary Fig. 3).

656

657 **Toxicity Study**

658 WT TIE-1 with an empty vector (pRhokS-2) was used to test the tolerance of TIE-1 for acetone
659 and *n*-butanol. To test the tolerance, 0%, 0.25%, 0.5%,1%, or 2% *n*-butanol (v/v), or 0%, 0.1%,
660 0.25%, 0.5%, 1%, or 2% acetone (v/v), was added to FW media with acetate (10 mM). Growth
661 was monitored by recording OD₆₆₀ over time.

662

663 **Statistics**

664 All statistical analyses (two tails Student's t-test) were performed with Python. *p*-value<0.05 was
665 considered to be significant. All the experiments were carried out using biological triplicates and
666 technical triplicates except for RT-qPCR for photoelectroautotrophy which was performed as
667 technical duplicates.

668

669 **Acknowledgments**

670 **General:** We thank the following members of the Washington University community: Marta
671 Wegorzewska and James Ballard for their careful reading of the manuscript; Dianne Duncan for
672 her help with confocal microscopy; and Dr. Joshua Blodgett, Dr. Michael Singh Guzman, Dinesh
673 Gupta, and Yunci Qi for their helpful comments during the preparation of this manuscript.

674

675 **Funding:** This work was supported by the following grants to A.B.: The David and Lucile Packard
676 Foundation Fellowship (201563111), the U.S. Department of Energy (grant number
677 DESC0014613;), and the U.S. Department of Defense, Army Research Office (grant number
678 W911NF-18-1-0037) , Gordon and Betty Moore Foundation, National Science
679 Foundation (Grant Number 2021822), and the U.S. Department of Energy by Lawrence
680 Livermore National Laboratory under Contract DEAC5207NA27344 (LLNL-JRNL-
681 812309). A.B. was also funded by a Collaboration Initiation Grant, an Office of the
682 ViceChancellor of Research Grant, and an International Center for Energy, Environment, and
683 Sustainability Grant from Washington University in St. Louis.

684

685 **Author contributions:** W.B., A.B., and K.R. designed the research. W.B, T.O.R., and K.R,
686 collected the data. W.B., T.O.R., and A.B. analyzed and interpreted the data. W.B., R.S., K.R. and
687 A.B. wrote the manuscript. All authors reviewed, revised, and approved the final manuscript.

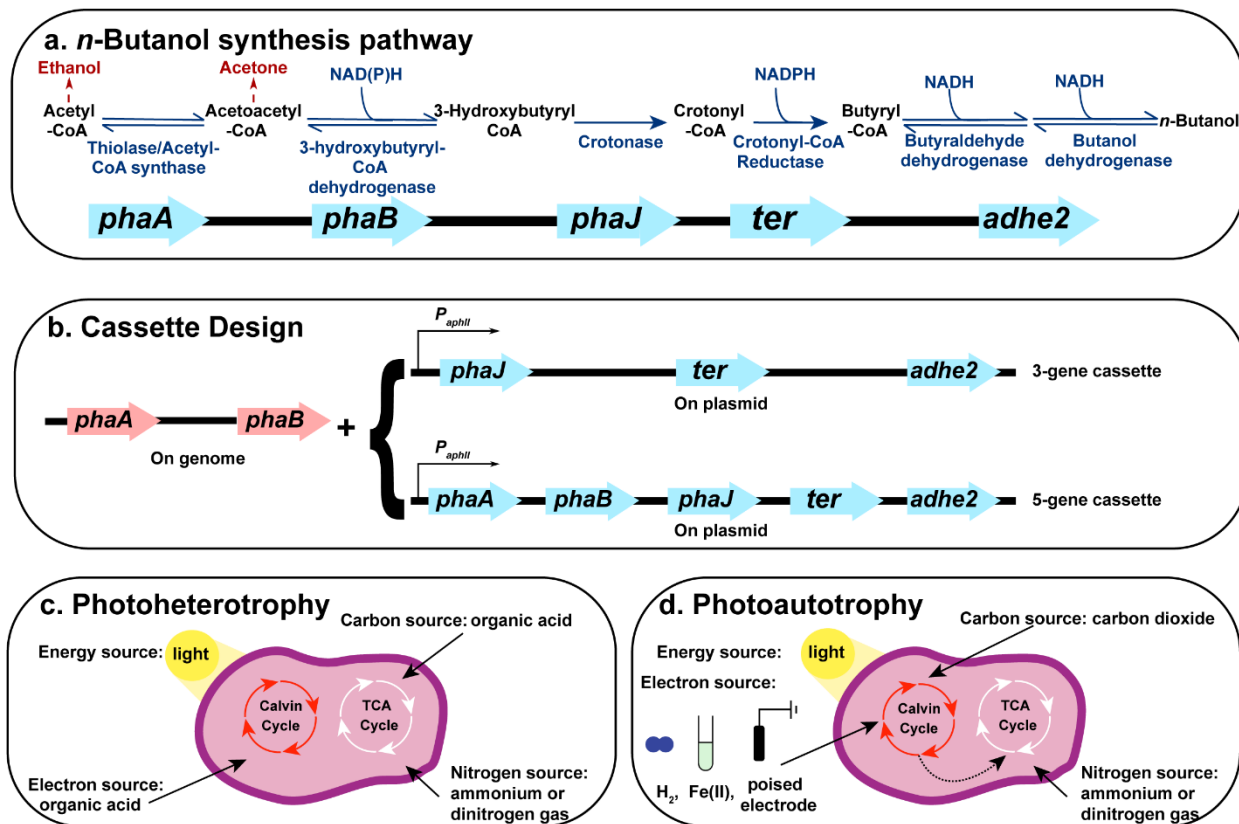
688

689 **Competing interests:** The authors declare no competing interests.

690

691 **Data and materials availability:** All data in this study are available from the corresponding
692 authors upon request.

693



694

695 **Figure 1. *n*-Butanol synthesis pathway, cassette design and major metabolisms used for *n*-butanol production**

696 **in *Rhodospseudomonas palustris* TIE-1. (a) *n*-butanol biosynthesis pathway involves five genes. The enzymes**

697 **encoded by each gene and the reactions catalyzed by these enzymes are shown in dark blue. Two major byproducts**

698 **(acetone and ethanol) are shown in dark red. NADH, nicotinamide adenine dinucleotide. (b) Cassette design. The 3-**

699 **gene cassette relies on *phaA* and *phaB* on the genome of TIE-1 for the first two steps of *n*-butanol synthesis. Here,**

700 **only 3-genes (*phaJ*, *ter*, and *adhE2*) were introduced on a plasmid under a constitutive promoter. The 5-gene**

701 **cassette has all five genes (*phaA*, *phaB*, *phaJ*, *ter*, and *adhE2*) on the plasmid under a constitutive promoter (c)**

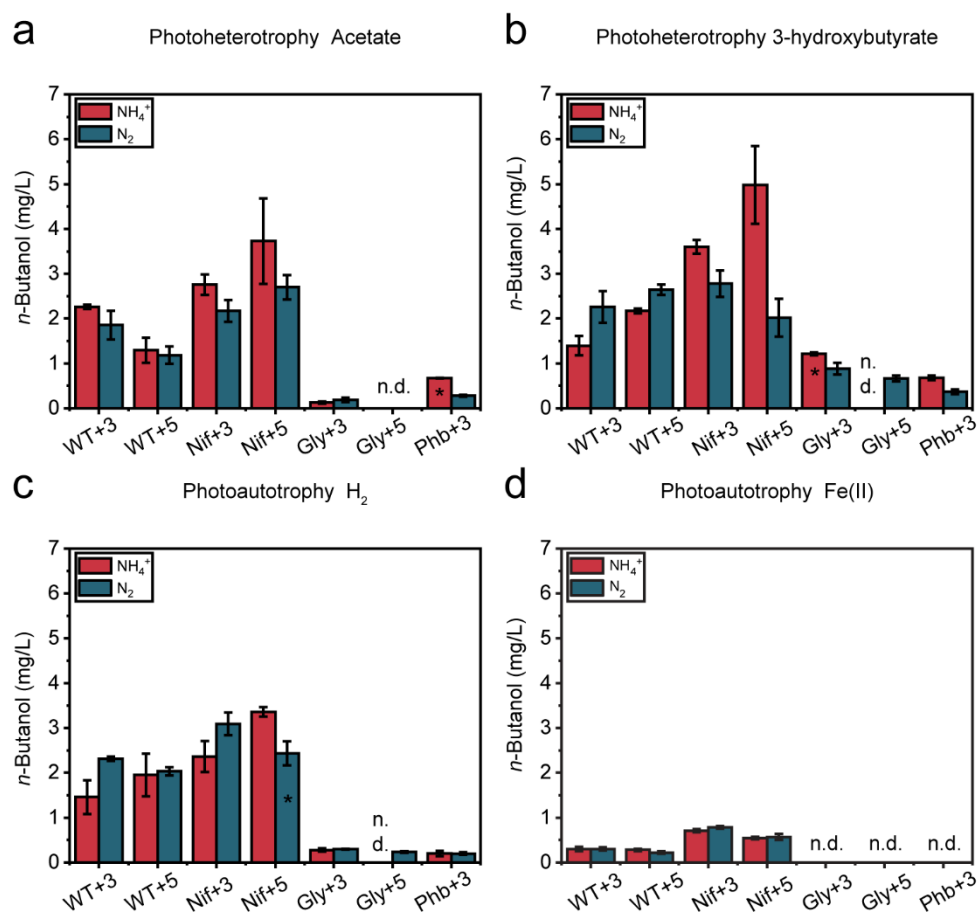
702 **Photoheterotrophy: TIE-1 uses organic acids as carbon and electron source, light as an energy source, and**

703 **ammonium or dinitrogen gas as a nitrogen source. (d) Photoautotrophy: TIE-1 uses carbon dioxide (CO₂) as carbon**

704 **source, hydrogen (H₂), ferrous iron (Fe(II)), or poised electrode as an electron source, light as an energy source, and**

705 **ammonium or dinitrogen gas as a nitrogen source**

706

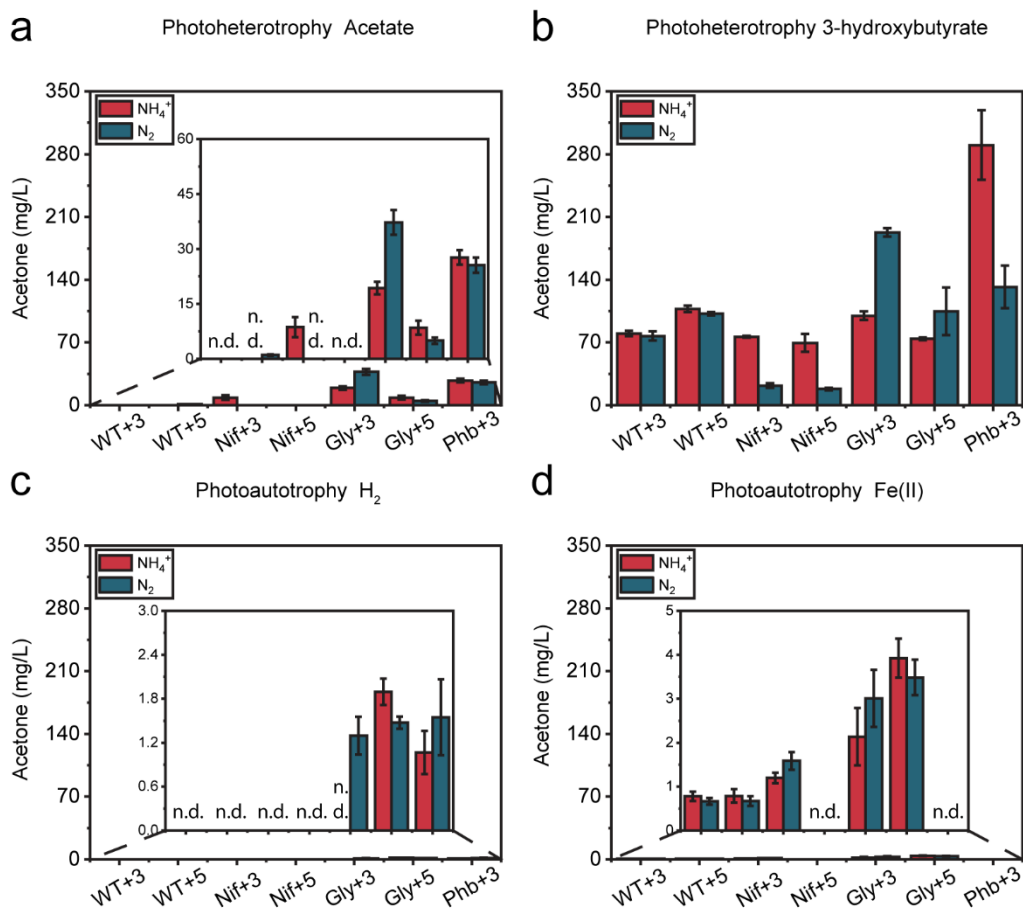


707

708

709 **Figure 2. The nitrogenase double mutant (Nif) produced the highest amount of *n*-butanol in the presence of 3-**
 710 **hydroxybutyrate.** The concentration of *n*-butanol in mg/L when TIE-1 was cultured with ammonium (NH₄⁺, red) or
 711 dinitrogen gas (N₂, blue) and (a) acetate (photoheterotrophy) (b) 3-hydroxybutyrate (photoheterotrophy) (c) hydrogen
 712 (H₂) (photoautotrophy) and (d) ferrous iron (Fe(II)) (photoautotrophy). CO₂ was present in all conditions. Data are
 713 means ± s.e.m. (standard error of the mean) of three biological replicates (bars that only have two biological replicates
 714 are indicated by '*') and three technical replicates. WT+3: wild type with 3-gene cassette; WT+5: wild type with 5-
 715 gene cassette; Nif+3: nitrogenase knockout t with 3-gene cassette; Nif+5: nitrogenase knockout with 5-gene cassette;
 716 Gly+3: glycogen synthase knockout with 3-gene cassette; Gly+5: glycogen synthase knockout with 5-gene cassette;
 717 Phb+3: hydroxybutyrate polymerase knockout with 3-gene cassette, n.d. (non-detectable).

718



719

720 **Figure 3. High *n*-butanol production correlates to low acetone production amongst TIE-1 mutants.** The

721 concentration of acetone in mg/L when TIE-1 was cultured with ammonium (NH₄⁺, red) or dinitrogen gas (N₂, blue)

722 and (a) acetate (photoheterotrophy) (b) 3-hydroxybutyrate (photoheterotrophy) (c) hydrogen (H₂) (photoautotrophy)

723 and (d) ferrous iron (Fe(II)) (photoautotrophy). CO₂ was present in all conditions. Data are means ± s.e.m. (standard

724 error of the mean) of three biological replicates and three technical replicates. WT+3: wild type with 3-gene cassette;

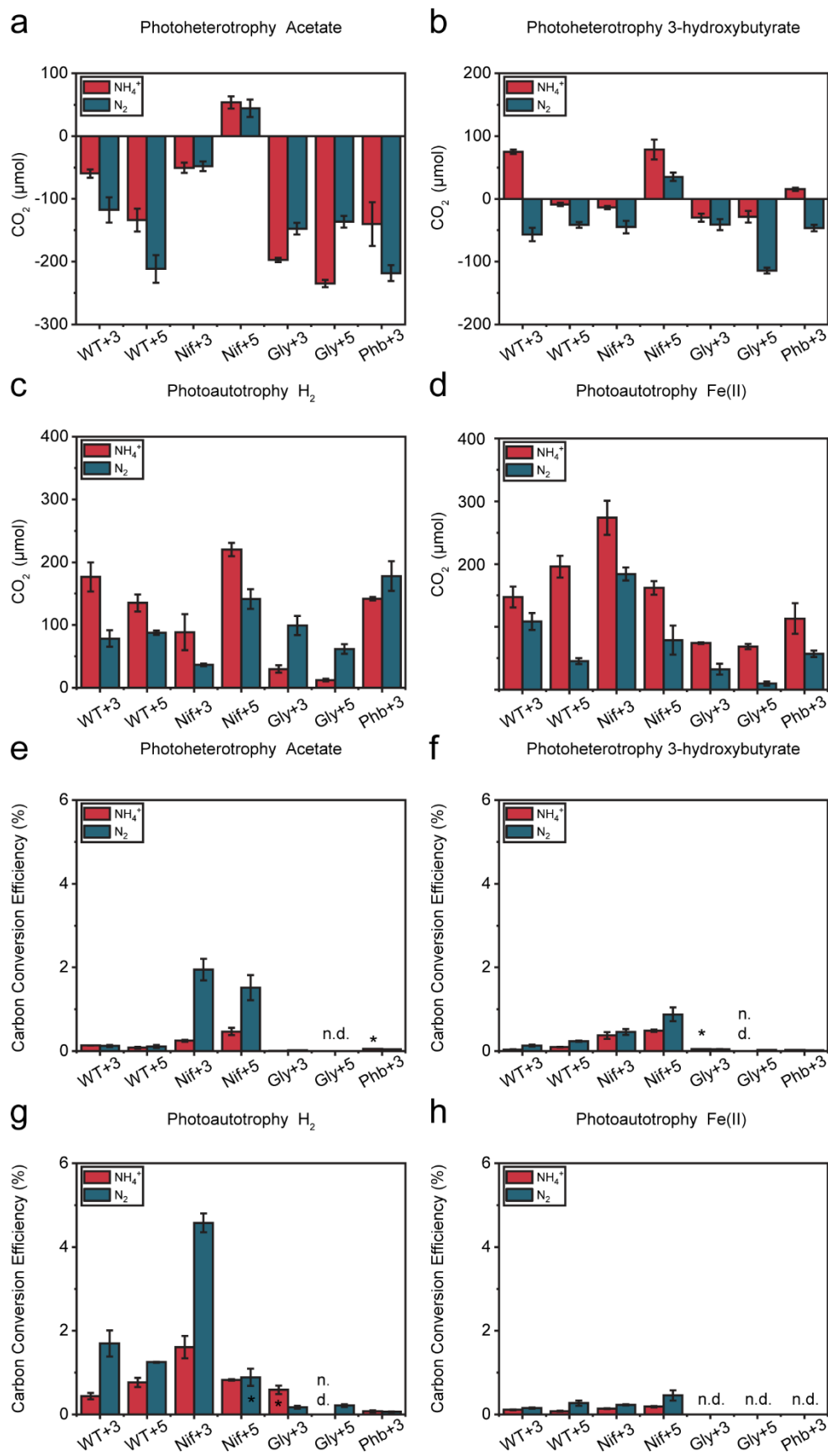
725 WT+5: wild type with 5-gene cassette; Nif+3: nitrogenase knockout t with 3-gene cassette; Nif+5: nitrogenase

726 knockout with 5-gene cassette; Gly+3: glycogen synthase knockout with 3-gene cassette; Gly+5: glycogen synthase

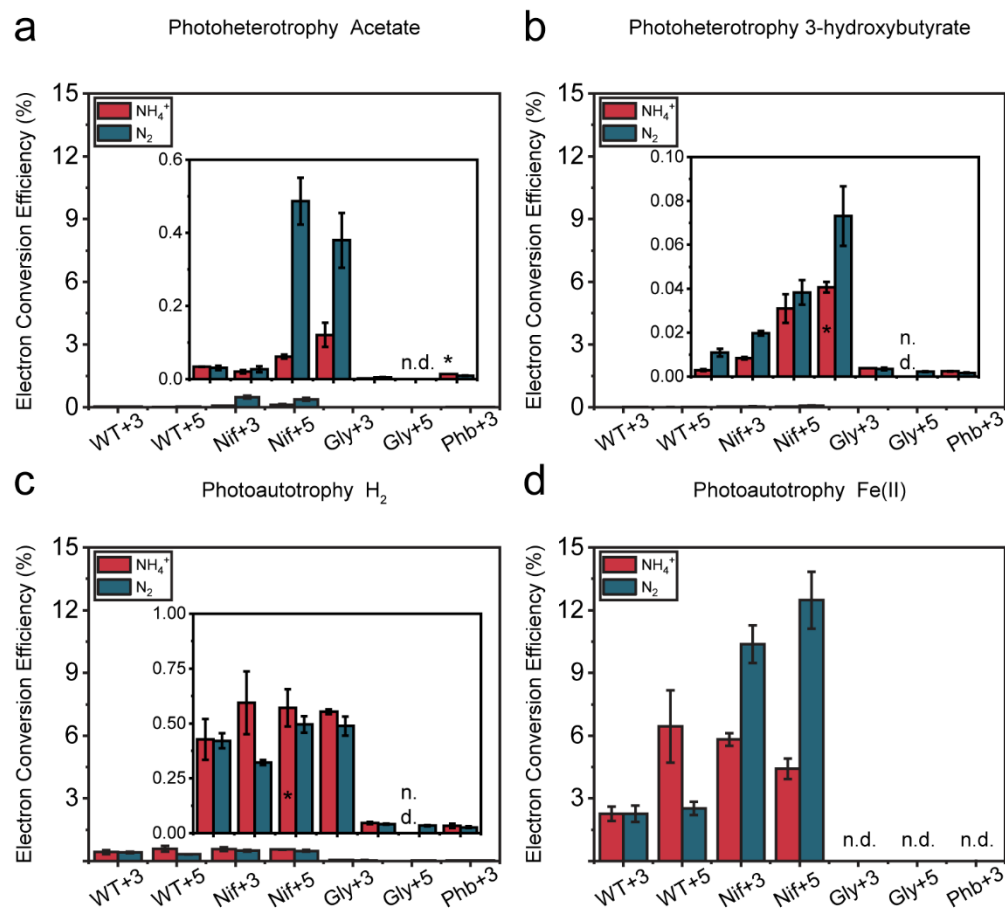
727 knockout with 5-gene cassette; Phb+3: hydroxybutyrate polymerase knockout with 3-gene cassette, n.d. (non-

728 detectable).

729



731 **Figure 4. The nitrogenase double mutant (Nif) converts carbon to *n*-butanol more efficiently.** (a)-(d): The CO₂
732 consumption (positive value)/production (negative value). (e)-(h): The percentage of carbon converted to *n*-butanol.
733 (a) and (e): acetate (photoheterotrophy) (b) and (f): 3-hydroxybutyrate (photoheterotrophy) (c) and (g): hydrogen (H₂)
734 (photoautotrophy) and (d) and (h): ferrous iron (Fe(II)) (photoautotrophy). CO₂ was present in all conditions. CO₂
735 was present in all conditions. Data are means ± s.e.m. (standard error of the mean) of three biological replicates (bars
736 that only have two biological replicates are indicated by '*') and three technical replicates. WT+3: wild type with 3-
737 gene cassette; WT+5: wild type with 5-gene cassette; Nif+3: nitrogenase knockout with 3-gene cassette; Nif+5:
738 nitrogenase knockout with 5-gene cassette; Gly+3: glycogen synthase knockout with 3-gene cassette; Gly+5: glycogen
739 synthase knockout with 5-gene cassette; Phb+3: hydroxybutyrate polymerase knockout with 3-gene cassette, n.d.
740 (non-detectable).
741
742



743

744 **Figure 5. The nitrogenase double mutant (Nif) converts electron to *n*-butanol more efficiently.** The electron

745 conversion efficiency (%) when TIE-1 was cultured with ammonium (NH₄⁺, red) or dinitrogen gas (N₂, blue) and (a)

746 acetate (photoheterotrophy) (b) (3-hydroxybutyrate (photoheterotrophy) (c) hydrogen (H₂) (photoautotrophy); and (d)

747 ferrous iron (Fe(II)) (photoautotrophy). CO₂ was present in all conditions. Data are means ± s.e.m. (standard error of

748 the mean) of three biological replicates (bars that only have two biological replicates are indicated by '*') and three

749 technical replicates. WT+3: wild type with 3-gene cassette; WT+5: wild type with 5-gene cassette; Nif+3: nitrogenase

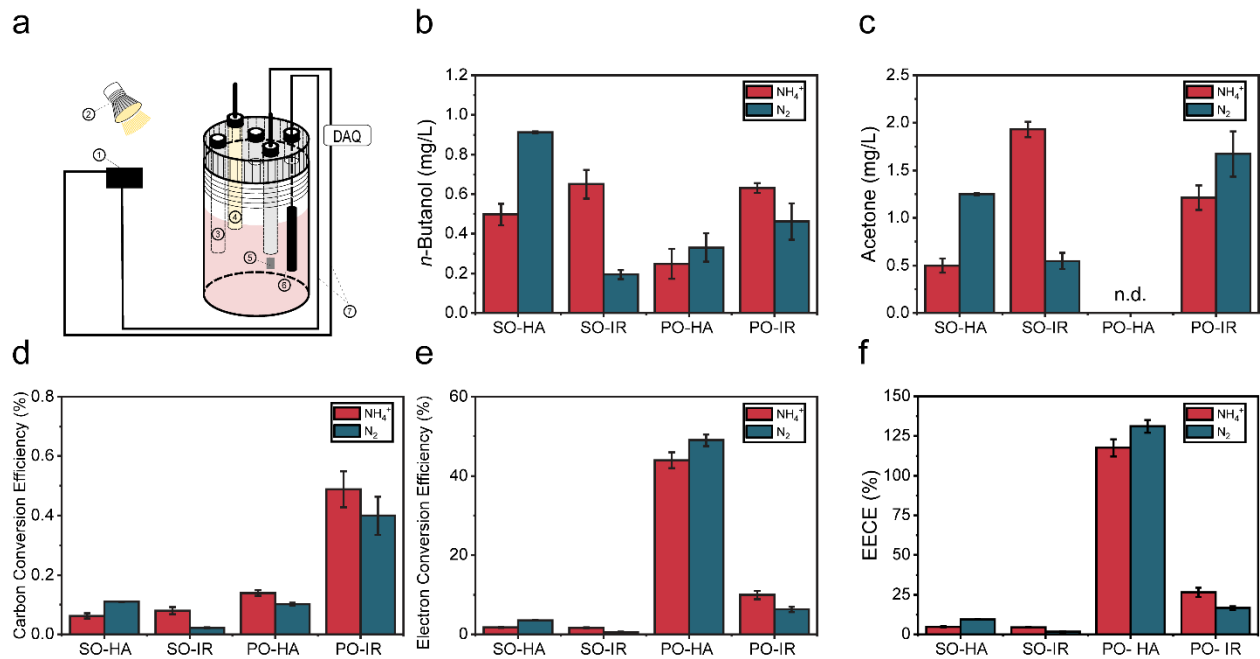
750 knockout t with 3-gene cassette; Nif+5: nitrogenase knockout with 5-gene cassette; Gly+3: glycogen synthase

751 knockout with 3-gene cassette; Gly+5: glycogen synthase knockout with 5-gene cassette; Phb+3: hydroxybutyrate

752 polymerase knockout with 3-gene cassette, n.d. (non-detectable).

753

754



755
 756 **Figure 6. *n*-Butanol production, acetone production carbon conversion efficiency, electron conversion**
 757 **efficiency and electrical energy conversion efficiency (EECE) by the nitrogenase double mutant with the 5-gene**
 758 **cassette under photoelectroautotrophy.** Under photoelectroautotrophic conditions, TIE-1 gains electrons from a
 759 poised electrode, using light as an energy source and carbon dioxide as a carbon source. For all the platforms, either
 760 ammonium (NH_4^+) or dinitrogen gas (N_2) was supplied. (a) Schematic set up of BEC platform. platform set up: 1-
 761 electricity source 2-light source, 3- Purge inlet, 4- Reference electrode (Ag/AgCl in 3M KCl), 5- Counter electrode
 762 (Pt foil, 5 cm^2), 6- Working electrode (Graphite rod, 3.2 cm^2), DAQ- Data acquisition); (b) *n*-butanol production; (c)
 763 acetone production; (d) carbon conversion efficiency; (e) electron conversion efficiency; (f) Electrical Energy
 764 conversion efficiency EECE (%). PO- potentiostat, IR- infrared light, HA: halogen light, SO: solar panel. Data are
 765 means \pm s.e.m. (standard error of the mean) of two biological replicates and three technical replicates.

766

767

768 References:

- 769 1 Woodwell, G. M. The warming of the industrialized middle latitudes 1985–2050: Causes
770 and consequences. *Climatic Change* **15**, 31-50, doi:10.1007/BF00138844 (1989).
- 771 2 Hofmann, D. J., Butler, J. H. & Tans, P. P. A new look at atmospheric carbon dioxide.
772 *Atmospheric Environment* **43**, 2084-2086, (2009).
- 773 3 Alalwan, H. A., Alminshid, A. H. & Aljaafari, H. A. S. Promising evolution of biofuel
774 generations. Subject review *Renewable Energy Focus* **28**, 127-139, (2019).
- 775 4 Dürre, P. Biobutanol: An attractive biofuel. *Biotechnology Journal* **2**, 1525-1534, (2007).
- 776 5 Trindade, W. R. D. S. & Santos, R. G. D. Review on the characteristics of butanol, its
777 production and use as fuel in internal combustion engines. *Renewable and Sustainable*
778 *Energy Reviews* **69**, 642-651, (2017).
- 779 6 Ndaba, B., Chiyanzu, I. & Marx, S. *n*-Butanol derived from biochemical and chemical
780 routes: A review. *Biological Reports* **8**, 1-9, (2015).
- 781 7 Jones, D. T. & Woods, D. R. Acetone-butanol fermentation revisited. *Microbiological*
782 *reviews* **50**, 484-524, (1986).
- 783 8 Atsumi, S. & Liao, J. C. Metabolic engineering for advanced biofuels production from
784 *Escherichia coli*. *Current Opinion in Biotechnology* **19**, 414-419, (2008).
- 785 9 Steen, E. J. *et al.* Metabolic engineering of *Saccharomyces cerevisiae* for the production
786 of *n*-butanol. *Microbial Cell Factories* **7**, 36, (2008).
- 787 10 Liu, W., Zhang, B. & Jiang, R. Improving acetyl-CoA biosynthesis in *Saccharomyces*
788 *cerevisiae* via the overexpression of pantothenate kinase and PDH bypass. *Biotechnology*
789 *for Biofuels* **10**, 97, (2017).
- 790 11 Nielsen, D. R., Leonard, E., Yoon, S., Tseng, H., Yuan, C. & Prather, K.L. Engineering
791 alternative butanol production platforms in heterologous bacteria. *Metabolic Engineering*
792 **11**, 262-273, (2009).
- 793 12 Ganigue, R., Puig, S., Batlle-Vilanova, P., Balaguer, M. D. & Colprim, J. Microbial
794 electrosynthesis of butyrate from carbon dioxide. *Chemical Communications* **51**, 3235-
795 3238, (2015).
- 796 13 Van der Woude, A. D., Angermayr, S. A., Puthan Veetil, V., Osnato, A. & Hellingwerf,
797 K. J. Carbon sink removal: Increased photosynthetic production of lactic acid by
798 *Synechocystis* sp. PCC6803 in a glycogen storage mutant. *Journal of Biotechnology* **184**,
799 100-102, (2014).
- 800 14 Lan, E. I. & Liao, J. C. Metabolic engineering of cyanobacteria for 1-butanol production
801 from carbon dioxide. *Metabolic Engineering* **13**, 353-363, (2011).
- 802 15 Lan, E. I. & Liao, J. C. ATP drives direct photosynthetic production of 1-butanol in
803 cyanobacteria. *Proceedings of the National Academy of Sciences* **109**, 6018, (2012).
- 804 16 Lan, E. I., Ro, S. Y. & Liao, J. C. Oxygen-tolerant coenzyme A-acylating aldehyde
805 dehydrogenase facilitates efficient photosynthetic *n*-butanol biosynthesis in
806 cyanobacteria. *Energy & Environmental Science* **6**, 2672-2681, (2013).
- 807 17 Liu, X., Miao, R., Lindberg, P. & Lindblad, P. Modular engineering for efficient
808 photosynthetic biosynthesis of 1-butanol from CO₂ in cyanobacteria. *Energy &*
809 *Environmental Science* **12**, 2765-2777, (2019).
- 810 18 Blankenship, R. E. *et al.* Comparing Photosynthetic and Photovoltaic Efficiencies and
811 Recognizing the Potential for Improvement. *Science* **332**, 805-809, (2011).

- 812 19 Liu, C., Colón, B. C., Ziesack, M., Silver, P. A. & Nocera, D. G. Water splitting–
813 biosynthetic system with CO₂ reduction efficiencies exceeding photosynthesis. *Science*
814 **352**, 1210-1213, (2016).
- 815 20 Abas, N., Kalair, E., Kalair, A., Hasan, Q. U. & Khan, N. Nature inspired artificial
816 photosynthesis technologies for hydrogen production: Barriers and challenges.
817 *International Journal of Hydrogen Energy* **45**, 20787-20799, (2020).
- 818 21 Aro, E.-M. From first generation biofuels to advanced solar biofuels. *Ambio* **45**, 24-31,
819 (2016).
- 820 22 Peralta-Yahya, P. P. & Keasling, J. D. Advanced biofuel production in microbes.
821 *Biotechnology Journal* **5**, 147-162, (2010).
- 822 23 Liu, C., Colón, B. E., Silver, P. A. & Nocera, D. G. Solar-powered CO₂ reduction by a
823 hybrid biological inorganic system. *Journal of Photochemistry and Photobiology A:
824 Chemistry* **358**, 411-415, (2018).
- 825 24 Clever, H. L. IUPAC Solubility Data Project 1973–2001. *Journal of Chemical &
826 Engineering Data* **49**, 1521-1529, (2004).
- 827 25 Horiuchi, J. I., Shimizu, T., Tada, K., Kanno, T. & Kobayashi, M. Selective production of
828 organic acids in anaerobic acid reactor by pH control. *Bioresource Technology* **82**, 209-
829 213, (2002).
- 830 26 Jiao, Y., Kappler, A., Croal, L. R. & Newman, D. K. Isolation and characterization of a
831 genetically tractable photoautotrophic Fe(II)-oxidizing bacterium, *Rhodopseudomonas
832 palustris* strain TIE-1. *Applied and Environmental Microbiology* **71**, 4487-4496, (2005).
- 833 27 Ranaivoarisoa, T. O., Singh, R., Rengasamy, K., Guzman, M. S. & Bose, A. Towards
834 sustainable bioplastic production using the photoautotrophic bacterium
835 *Rhodopseudomonas palustris* TIE-1. *Journal of Industrial Microbiology &
836 Biotechnology*, **46**, 1401–141,7 (2019).
- 837 28 Jeong, C. & Han, C. Byproduct hydrogen network design using pressure swing
838 adsorption and recycling unit for the petrochemical complex. *Industrial & Engineering
839 Chemistry Research* **50**, 3304-3311, (2011).
- 840 29 Bose, A., Gardel, E. J., Vidoudez, C., Parra, E. A. & Girguis, P. R. Electron uptake by
841 iron-oxidizing phototrophic bacteria. *Nature Communications* **5**, 3391, (2014).
- 842 30 Guzman, M. S. *et al.* Phototrophic extracellular electron uptake is linked to carbon
843 dioxide fixation in the bacterium *Rhodopseudomonas palustris*. *Nature Communications*
844 **10**, 1355, (2019).
- 845 31 Karthikeyan, R., Singh, R. & Bose, A. Microbial electron uptake in microbial
846 electrosynthesis: a mini-review. *J Ind Microbiol Biotechnol*, **46**, 1419–1426, (2019).
- 847 32 Doud, D. F. R. & Angenent, L. T. Toward electrosynthesis with uncoupled extracellular
848 electron uptake and metabolic growth: enhancing current uptake with
849 *Rhodopseudomonas palustris*. *Environmental Science & Technology Letters* **1**, 351-355,
850 (2014).
- 851 33 Doud, D. F. R., Holmes, E. C., Richter, H., Molitor, B., Jander, G. & Angenent, L.T..
852 Metabolic engineering of *Rhodopseudomonas palustris* for the obligate reduction of *n*-
853 butyrate to *n*-butanol. *Biotechnology for Biofuels* **10**, 11669, (2017).
- 854 34 Bond-Watts, B. B., Bellerose, R. J. & Chang, M. C. Y. Enzyme mechanism as a kinetic
855 control element for designing synthetic biofuel pathways. *Nature Chemical Biology* **7**, 1-
856 6, (2011).

- 857 35 Anfelt, J. *et al.* Genetic and nutrient modulation of acetyl-CoA levels in *Synechocystis*
858 for *n*-butanol production. *Microbial Cell Factories* **14**, 167, (2015).
- 859 36 Li, X., Shen, C. R. & Liao, J. C. Isobutanol production as an alternative metabolic sink to
860 rescue the growth deficiency of the glycogen mutant of *Synechococcus elongatus* PCC
861 7942. *Photosynthesis Research* **120**, 301-310, (2014).
- 862 37 Öztürk, Y. *et al.* Hydrogen production by using *Rhodobacter capsulatus* mutants with
863 genetically modified electron transfer chains. *International Journal of Hydrogen Energy*
864 **31**, 1545-1552, (2006).
- 865 38 McKinlay, J. B. & Harwood, C. S. Carbon dioxide fixation as a central redox cofactor
866 recycling mechanism in bacteria. *Proceedings of the National Academy of Sciences* **107**,
867 11669, (2010).
- 868 39 Huang, J. J., Heiniger, E. K., McKinlay, J. B. & Harwood, C. S. Production of hydrogen
869 gas from light and the inorganic electron donor thiosulfate by *Rhodospseudomonas*
870 *palustris*. *Appl Environ Microbiol* **76**, 7717-7722, (2010).
- 871 40 McNeil, B. & Kristiansen, B. The acetone butanol fermentation. *Advances in applied*
872 *Microbiology* **31**, 61-92, (1986).
- 873 41 McKinlay, J. B. & Harwood, C. S. Calvin cycle flux, pathway constraints, and substrate
874 oxidation state together determine the H₂ biofuel yield in photoheterotrophic bacteria.
875 *mBio* **2**, (2011).
- 876 42 Thiel, S., Döhring, T., Köfferlein, M., Kosak, A., Martin, P. & K.Seidlitz, H.. A
877 Phytotron for plant stress research: how far can artificial lighting compare to natural
878 sunlight? *Journal of Plant Physiology* **148**, 456-463, (1996).
- 879 43 Mohamad, T., Moria, H. & Aldawi, F. Radiation distribution uniformization by
880 optimized halogen lamps arrangement for a solar simulator. *The Journal of Scientific and*
881 *Engineering Research* **3**, 29-34 (2016).
- 882 44 White, D. *The Physiology and Biochemistry of Prokaryotes*. (Oxford Press,
883 Oxford,2007).
- 884 45 Sang Kim, J., Ito, K. & Takahashi, H. The relationship between nitrogenase activity and
885 hydrogen evolution in *Rhodospseudomonas palustris*. *Agricultural and Biological*
886 *Chemistry* **44**, 827-833, (1980).
- 887 46 Shen, C. R., Ethan, I. L., Yasumasa, D., Antonino, B., Kwang, M. C., James C. L.
888 Driving forces enable high-titer anaerobic 1-butanol synthesis in *Escherichia coli*.
889 *Applied and environmental microbiology* **77**, 2905-2915, (2011).
- 890 47 Hartmann, A., Fu, H. & Burris, R. H. Regulation of nitrogenase activity by ammonium
891 chloride in *Azospirillum* spp. *Journal of Bacteriology* **165**, 864-870, (1986).
- 892 48 Seefeldt, L. C., Hoffman, B. M. & Dean, D. R. Electron transfer in nitrogenase catalysis.
893 *Curr. Opin. Chem. Biol.* **16**, 19-25, (2012).
- 894 49 Dixon, R. & Kahn, D. Genetic regulation of biological nitrogen fixation. *Nat. Rev.*
895 *Microbiol.* **2**, 621-631, (2004).
- 896 50 Buehler, E. A. & Mesbah, A. Kinetic study of acetone-butanol-ethanol fermentation in
897 continuous culture. *PloS one* **11**, e0158243, (2016).
- 898 51 Posada, J. A., Naranjo, J. M., López, J. A., Higueta, J. C. & Cardona, C. A. Design and
899 analysis of poly-3-hydroxybutyrate production processes from crude glycerol. *Process*
900 *Biochemistry* **46**, 310-317, (2011).

- 901 52 Newcomer, A., Blumsack, S. A., Apt, J., Lave, L. B. & Morgan, M. G. Short run effects
902 of a price on carbon dioxide emissions from U.S. electric generators. *Environmental*
903 *Science & Technology* **42**, 3139-3144, (2008).
- 904 53 Uyttebroek, M., Van Hecke, W. & Vanbroekhoven, K. Sustainability metrics of 1-
905 butanol. *Catalysis Today* **239**, 7-10, (2015).
- 906 54 Li, X., Shi, Z. & Li, Z. Increasing butanol/acetone ratio and solvent productivity in ABE
907 fermentation by consecutively feeding butyrate to weaken metabolic strength of butyrate
908 loop. *Bioprocess Biosyst. Eng.* **37**, 1609-1616, (2014).
- 909 55 Rabanal-Arabach, J., Schneider, A. & Cabrera, E. Minimization of electrical losses of PV
910 modules located in places with high solar irradiance. *Energy Procedia* **77**, 402-406,
911 (2015).
- 912 56 Berginski, M. *et al.* Experimental studies and limitations of the light trapping and optical
913 losses in microcrystalline silicon solar cells. *Solar Energy Materials and Solar Cells* **92**,
914 1037-1042, (2008).
- 915 57 Polman, A., Knight, M., Garnett, E. C., Ehrler, B. & Sinke, W. C. Photovoltaic materials:
916 present efficiencies and future challenges. *Science* **352**, aad4424, (2016).
- 917 58 Andreani, L. C., Bozzola, A., Kowalczewski, P., Liscidini, M. & Redorici, L. Silicon
918 solar cells: toward the efficiency limits. *Advances in Physics: X* **4**, 1548305, (2019).
- 919 59 Zhang, B. & Sun, L. Artificial photosynthesis: opportunities and challenges of molecular
920 catalysts. *Chemical Society Reviews* **48**, 2216-2264, (2019).
- 921 60 Ohunakin, O. S., Adaramola, M. S., Oyewola, O. M. & Fagbenle, R. O. Solar energy
922 applications and development in Nigeria: drivers and barriers. *Renewable and*
923 *Sustainable Energy Reviews* **32**, 294-301, (2014).
- 924 61 Atsumi, S. *et al.* Metabolic engineering of *Escherichia coli* for 1-butanol production.
925 *Metabolic Engineering* **10**, (2008)
- 926 62 Schadeweg, V. & Boles, E. Increasing *n*-butanol production with *Saccharomyces*
927 *cerevisiae* by optimizing acetyl-CoA synthesis, NADH levels and trans-2-enoyl-CoA
928 reductase expression. *Biotechnology for Biofuels* **9**, 257, (2016).
- 929 63 Singh, R., Ranaivoarisoa, T. O., Gupta, D., Bai, W. & Bose, A. Genetic redundancy in
930 iron and manganese transport in the metabolically versatile bacterium
931 *Rhodospseudomonas palustris* TIE-1. *Applied and Environmental Microbiology*. **86**,
932 e01057-20, (2020).
- 933 64 Rengasamy, K., Ranaivoarisoa, T., Singh, R. & Bose, A. An insoluble iron complex
934 coated cathode enhances direct electron uptake by *Rhodospseudomonas palustris* TIE-1.
935 *Bioelectrochemistry* **122**, 164-173, (2018).
- 936 65 Rengasamy, K., Ranaivoarisoa, T., Bai, W. & Bose, A. A. Magnetite nanoparticle
937 anchored graphene cathode enhances microbial electrosynthesis of polyhydroxybutyrate
938 by *Rhodospseudomonas palustris* TIE-1. *Nanotechnology* (2020).
- 939 66 Fontaine, L., Meynial-Salles, I., Girbal, L., Yang, X., Croux, C & Soucaille, P.. Molecular
940 characterization and transcriptional analysis of adhE2, the gene encoding the NADH-
941 dependent aldehyde/alcohol dehydrogenase responsible for butanol production in
942 alcohologenic cultures of *Clostridium acetobutylicum* ATCC 824. *Journal of*
943 *Bacteriology* **184**, 821-830 (2002).
- 944 67 Tenny K.M., C. J. S. *Ideal Gas Behavior.*, (StatPearls Publishing, USA, 2020).
945

946 68 J. Speicht, M.-H. Lange's Handbook of Chemistry, 70th Anniversary Edition. (McGraw-
947 Hill Education, USA, 2005).
948
949